Modelling interacting cracks through a level set using the element-free Galerkin method

Muthu, N., Maiti, S. K., Yan, W., & Falzon, B. G. (2017). Modelling interacting cracks through a level set using the element-free Galerkin method. *International Journal of Mechanical Sciences*, *134*, 203-215. https://doi.org/10.1016/j.ijmecsci.2017.10.009

Published in:
International Journal of Mechanical Sciences

Document Version:
Peer reviewed version

Modelling interacting cracks through a level set using the element-free Galerkin method

N. Muthu[a,b], S.K. Maiti[c*], W. Yan[d,] B.G. Falzon[e*],

[a] *IITB-Monash Research Academy, CSE Building, 2nd Floor, IIT Bombay, Powai, 400076, India*
[b] *Department of Mechanical Engineering, IIT Guwahati, Guwahati, 781039, India*
[c] *Department of Mechanical Engineering, IIT Bombay, Powai, 400076, India*
[d] *Department of Mechanical and Aerospace Engineering, Monash University, Clayton, VIC 3800, Australia*
[e] *School of Mechanical and Aerospace Engineering, Queen's University Belfast, Belfast, BT9 5AH, UK*

ABSTRACT

A multiple crack weight technique with a level set method is proposed to model multiple cracks using a coarse mesh-free nodal discretization. A new level-set structure is presented to handle multiple cracks and their propagation using the maximum tangential principal stress criterion. The level sets are updated with respect to the new crack tip positions. The problem of modelling interacting cracks in isotropic and bi-materials is studied using a new variant of the element-free Galerkin method. The stress intensity factors (SIFs) and energy release rates for interacting cracks in isotropic and homogenous materials, including a crack at a bi-material interface are determined using the standard interaction integral. Case studies involving crack-crack interactions, doubly and triply kinked cracks are analyzed to demonstrate the simplicity and the effectiveness of the proposed approach.

KEY WORDS: Element-free Galerkin method, multiple cracks, level set method, crack-crack interaction, interface cracks, stress intensity factor

1. INTRODUCTION

Multiple cracks originate in close proximity due to stress corrosion cracking [1,2], creep [3], thermal fatigue, and may occur in, for example, lap joints and rivets [4], power plant components and nuclear power plant cooling systems [5]. An accurate assessment of life prediction requires the determination of the stress intensity factors (SIFs) under such situations.

Although the finite element method (FEM) and boundary element method (BEM) are often used to model interacting cracks, they require extensive meshing in the region consisting of multiple crack tips. In the case of a propagating crack, singularities occur at re-entrant corners and at a crack tip. This makes the re-meshing computationally costly. To overcome this problem with meshing, special elements like quarter point [6], variable order [7] and multi-point [8,9] singularity elements have been implemented in FEM. Subsequently, the extended finite element method (XFEM) [10,11] eliminated some of the difficulties associated with meshing and re-meshing. Nevertheless, the enrichment functions used in this method are also dependent on the material and nature of the crack considered. To make the method independent of material, orientation of crack and loading, the generalized finite element method (GFEM) [12] was introduced where a local solution obtained from global-local analysis was used as the enrichment function. Meanwhile, meshfree methods (MMs) have gained popularity in the analysis of crack propagation problems. The shape functions of the MMs are generally higher

order continuous [13] than that of the FEM. Therefore, unlike mesh-based methods, MMs do not require extensive discretization to capture the singular field at the crack tip.

The element-free Galerkin (EFG) method [14,15,16,17], one of the popular formulations in MMs, is used in the present work. There are two popular approaches to model the crack: (1) The partition-of-unity approach, also known as the eXtended element-free Galerkin (XEFG) method [18], based on the XFEM, where additional degrees of freedom are introduced to model the crack; and (2) where the weight functions of the nodes, whose domain of influence consists of the crack tips, are modified. Some of the methods based on the latter approach are: visibility method, diffraction method and transparency method. In this work, a combined method [19] is used, which consists of the partition-of-unity approach, to model the discontinuity in the crack faces using a Heaviside function, and the diffraction method to modify the weight function to model the crack tip.

Duflot et al. [20,21] modelled multiple cracks by multiplying the regular weight functions with the square root of the distance from the crack tip. Singh et al. [22] proposed a modified intrinsic meshfree method for modelling multiple cracks. They biased the enrichment by the proximity of the Gauss point to a particular crack tip. Shi et al. [23] demonstrated the accurate modelling of the interacting cracks using the partition-of-unity based EFG method. The enrichment functions used in the approaches above are dependent on the crack geometry and material properties. Modelling an interface crack or a re-entrant corner/wedge crack interacting with other cracks requires significant alteration using the above formulations. The distance-based enriched weight function method, developed by Barbieri et al. [24], overcomes some of the difficulties with the other formulations. However, they did not validate their method for interacting cracks. The multiple crack weight (MCW) technique was introduced by Muravin & Turkel [25] to model multiple interacting cracks. Calculating the parameters of this MCW technique is difficult in the presence of many arbitrary oriented cracks.

Level set method (LSM) was developed by Osher et al. [26] for modelling the motion of interfaces. It has been used for a wide range of applications [27] such as image processing, computational geometry, optimization, computational fluid dynamics and computer graphics. LSM has been used to represent the crack location including the location of crack tips within the context of XFEM [28]. The combination of LSM and numerical methods such as XFEM and MMs provided a simple way of modelling crack growth in two and three dimensions [29]. Any surface of discontinuity, in this case a crack, is represented by a signed distance function that is determined by a set of nodes. As the crack propagates, the level set function is updated by an evolution equation [30,31,32]. Usually, MMs nodes themselves act as nodes to store level set functions. This removes the need for explicitly representing a crack. In this work, a background grid consisting of finer discretized nodes are defined to store the vector level set corresponding to a crack. Simple algebraic equations are used to update the vector level-set function in the background nodes.

In this work, the modified MCW technique is used in conjunction with the vector level sets to model the interaction of multiple cracks using the proposed EFG method. This technique is broadened to model kinked cracks that involve re-entrant corners/knee singularity. A general procedure that uses a recursive function to model many cracks using the diffraction method is described. To demonstrate the efficiency and accuracy of the proposed approach, case studies involving multiple crack interactions, crack-microcrack interactions, interface crack-microcrack, double and triple kinked cracks have been solved. All cases are investigated using linear elastic fracture mechanics (LEFM) principles. There exist many SIF extraction techniques [33,34] within the framework of MMs; the M-integral/interaction integral is used in this work to compute the SIFs. The results are compared with existing results in the literature.

The aspect of shielding and amplification of the energy release rate (ERR) for a crack interacting with a microcrack is also presented.

2. DISCONTINUITY MODELLING USING MODIFIED EFG METHOD

In the displacement-based EFG method, the displacement at location $\mathbf{x}$ within a support domain of n nodes, $\mathbf{u}(\mathbf{x})$, can be represented as

$$\mathbf{u}(\mathbf{x}) = \sum_{\mathrm{I}=1}^{\mathrm{n}} \Phi_{\mathrm{I}}(\mathbf{x})\mathbf{u}_{\mathrm{I}} \tag{1}$$

where $\Phi_{\mathrm{I}}(\mathbf{x})$ are the nodal shape functions and $\mathbf{u}_{\mathrm{I}}$ are the nodal displacement vectors. The shape functions are developed using the moving least squares (MLS) interpolation technique [35]. In this work, the crack tip is modelled using the diffraction method. The region away from the crack tip is modelled with a Heaviside function to introduce displacement discontinuity across the crack faces as shown in Fig. 1. This eliminates the need of special enrichment functions that are problem dependent [36].

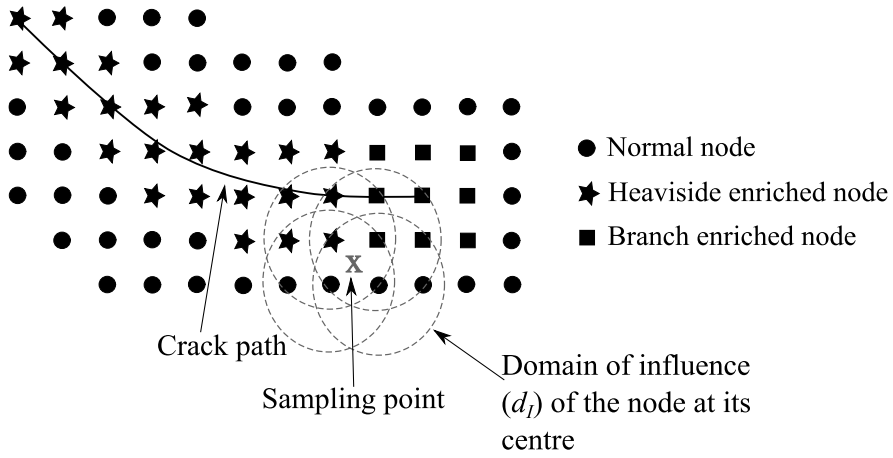

Fig. 1. Nodal discretization with enriched nodes in the region around the crack tip.

Accordingly, the displacement approximation in the proposed EFG method in the case of a crack (strong discontinuity) and inclusion boundary (weak discontinuity) present in a representative geometry (Fig. 2), takes the form of,

$$\mathbf{u}(\mathbf{x}) = \sum_{I\in w(\mathbf{x})} \Phi_I(\mathbf{x})\mathbf{u}_I + \sum_{I\in w_j(\mathbf{x})} \Phi_I(\mathbf{x})\{\mathbf{a}_I \mathrm{H}(f(\mathbf{x}))\} + \sum_{I\in w_b(\mathbf{x})} \Phi_I(\mathbf{x})\mathbf{b}_I \chi_I(\mathrm{x}) \tag{2}$$

where the function $\chi_I(\mathrm{x}) = \mathrm{F}^{\mathrm{I}}(\mathrm{x}) - \mathrm{F}^{\mathrm{I}}(\mathrm{x}_I)$, is employed for displacement continuity across the interface, with $\mathrm{F}^{\mathrm{I}}(\mathrm{x}) = \sum_{I\in w_c(\mathrm{x})} |\zeta_I| \Phi_I(x) - \left| \sum_{I\in w_c(\mathrm{x})} \zeta_I \Phi_I(x) \right|$. ζ_I is the signed distance of node I from the interface. $\mathbf{a}_I$ and $\mathbf{b}_I$ are nodal enriched degrees-of-freedom associated with the Heaviside function and level set function [36] respectively. The set $w_j(\mathbf{x})$ and $w_b(\mathbf{x})$ consist of the Heaviside enriched and level set enriched nodes with a displacement continuity function.

In the case of a geometry with n_c cracks and n_m material interfaces, the displacement $\mathbf{u}(\mathbf{x})$ is given by

$$\mathbf{u}(\mathbf{x}) = \sum_{I\in w(\mathbf{x})} \Phi_I(\mathbf{x})\mathbf{u}_I + \sum_{n=1}^{n_c} \sum_{I\in w_j(\mathbf{x})} \Phi_I^n(\mathbf{x})\{\mathbf{a}_I^n \mathrm{H}(f^n(\mathbf{x}))\} + \sum_{n=1}^{n_m} \sum_{I\in w_b(\mathbf{x})} \Phi_I^n(\mathbf{x})\mathbf{b}_I^n \chi_I(\mathrm{x}) \tag{3}$$

The proposed variant of the EFG method can be used to model any number of cracks and is not

limited by the type of material, loading or orientation of the cracks. To improve the accuracy of the numerical method, a higher order Gauss integration is used in the background triangular cells [19].

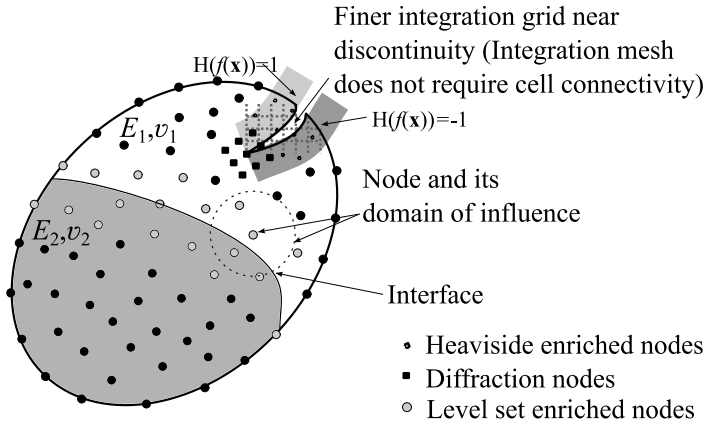

Fig. 2. Nodal discretization for a domain with a crack in a bi-material problem.

3. REFORMULATION OF MULTIPLE CRACK WEIGHT (MCW) FUNCTION

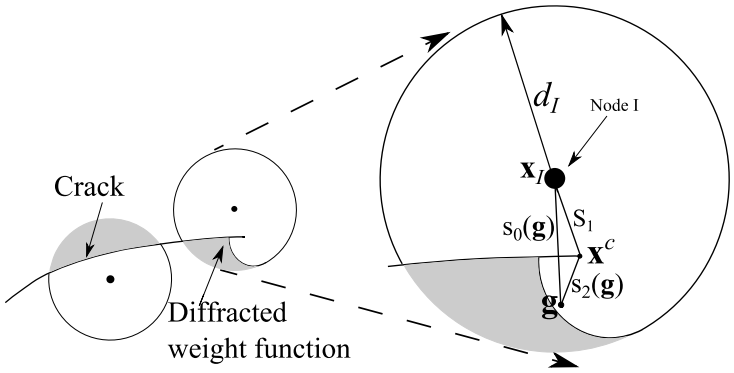

Fig. 3 Diffraction method for a single crack.

The diffraction method [13,16,19,34] is one of the ways of modelling a crack using the EFG method. This method is based on the analogy that light diffracts around sharp corners. Here, the weight function of a node that has a crack tip in its domain (d_I), has its influence over a region dictated by the diffraction space associated with a point 'light' source at the node and the crack acting as an opaque object. This ensures the generation of smooth shape functions, which in turn yield a smooth strain field. An important aspect of the method is to find the shortest distance between the source node and a generic point. In the case of a single crack (Fig. 3), depending on a generic point location, $\mathbf{g}(x, y)$, the location of the crack tip, $\mathbf{x}^c$, and the nodal location, $\mathbf{x}_I$, the distance, d_r, between $\mathbf{x}_I$ and $\mathbf{g}$ is modified by the relation

$$d_r = \left(\frac{s_1 + s_2(\mathbf{g})}{s_0(\mathbf{g})} \right)^{\lambda} s_0(\mathbf{g}) \tag{4}$$

where $s_0(\mathbf{g}) = \|\mathbf{g} - \mathbf{x}_I\|$. A value of 2 is chosen for parameter λ. s_1 is the distance from the node I at location $\mathbf{x}_I$ to $\mathbf{x}^c$. $s_2(\mathbf{g})$ is the distance from $\mathbf{x}^c$ to $\mathbf{g}$. In all case studies in this presented paper, a cubic weight function [13,34], $w(r)$, is used,

$$w(r) = \begin{cases} 2/3 - 4r^2 + 4r^3, r \le 0.5 \\ 4/3 - 4r + 4r^2 - 4/3r^3, 0.5 < r \le 1 \\ 0, r > 1 \end{cases} \tag{5}$$

where $r = d_r / d_I$. The surface plot of the cubic spline function is shown in Fig. 4.

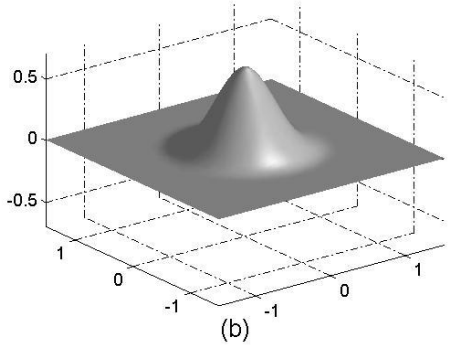

Fig. 4 Cubic spline weight function.

Because of Eq. (4), the normal circular domain of influence is truncated as shown in Fig. 3. The shadow region, where $w(r) = 0$, near the crack is caused by the higher values of d_r i.e. $d_r > 1$. d_r will be equal to $\mathrm{s}_0(\mathbf{g})$ if the line-of-sight (LOS) from $\mathbf{x}_I$ to $\mathbf{g}$ is not obstructed by the crack.

When multiple cracks are located in close proximity, it is necessary to use very high refinement to ensure that no two (or multiple) crack tips are influenced by a single node. On the other hand, the MCW technique enables coverage for multiple crack tips by a single node, mitigating the need for high nodal density. Modelling multiple crack tips through the diffraction method is possible because of the higher order continuous nature of the EFG shape functions derived using the MLS approach.

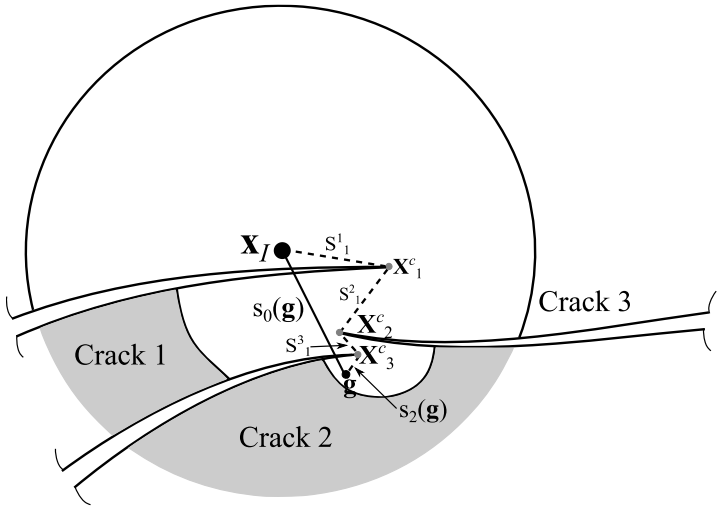

Fig. 5 Multiple crack weight (MCW) technique.

Fig. 5 shows a case of multiple interacting cracks where all the crack tips are located within d_I of a node *I* whose weight function is diffracted around each of the crack tips. In the MCW technique, s_1 in Eq. (4) is modified by

$$
\begin{aligned}
\mathrm{s}_1 &= \sum_{n_c=1}^{n} \mathrm{s}_1^{n_c} \\
\mathrm{s}_1^{n_c} &= \begin{cases} \left\| \mathbf{x}_1^c - \mathbf{x}_I \right\|, & n_c = 1 \\ \left\| \mathbf{x}_{n_c}^c - \mathbf{x}_{n_c-1}^c \right\|, & n_c \neq 1 \end{cases} \\
\mathrm{s}_2(\mathbf{g}) &= \left\| \mathbf{g} - \mathbf{x}_{n_c}^c \right\|
\end{aligned}
\tag{6}
$$

where $\mathbf{x}_{n_c}^c$ is the location of crack tip n_c $(1 \le n_c \le n)$. n is the total number of cracks whose tips are influenced by the node I. For instance, in Fig. 5, $\mathrm{s}_1 = \mathrm{s}_1^1 + \mathrm{s}_1^2 + \mathrm{s}_1^3$ and $\mathrm{s}_2(\mathbf{g}) = \left\| \mathbf{g} - \mathbf{x}_3^c \right\|$. This definition is slightly different from what was used by Muravin and Turkel [25].

$\mathrm{s}_1 + \mathrm{s}_2(\mathbf{g})$ is the shortest path from the node to a sampling point $\mathbf{g}$. s_1 is the distance from the node to the closest intercepting crack tip location and $\mathrm{s}_2(\mathbf{g})$ is the distance from that crack tip to the Gauss point. A method to compute the parameters s_1 and $\mathrm{s}_2(\mathbf{g})$ is presented in the following section. This is facilitated by the level set method, adopted for MMs to help study the problem of modelling multiple cracks and their propagation.

4. LEVEL SET METHOD FOR 2D CRACK

The level set method is used to represent the crack location. This is facilitated by a signed distance function $f(\mathbf{x})$, which contains the signed normal distance from a grid point $\mathbf{x}$ to the crack. A crack is represented as a zero level set of the function, $f(\mathbf{x})$, Fig. 6. The end points of the crack, i.e. crack tip locations, are kept in store separately.

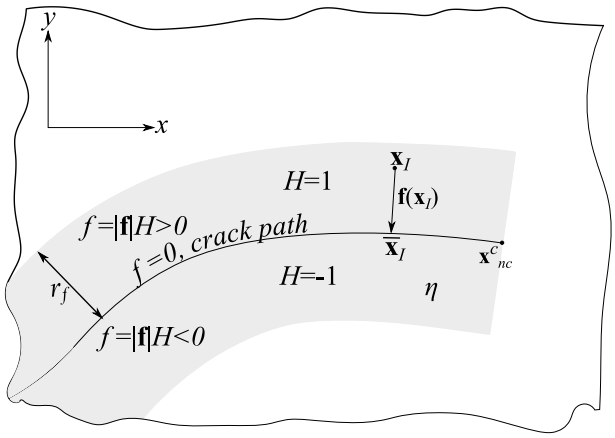

Fig. 6 Level set description for a crack.

The sign of the level set function, $f(\mathbf{x})$, is +ve if $\mathbf{x}$ lies above the crack and –ve if it lies below the crack. The sign information is given by $H(f(\mathbf{x}))$ where H is the Heaviside function. Since the area of interest is localized to the crack, the level set computations are restricted to the region that surrounds the crack. This region is called a 'narrow band' and is indicated in grey (Fig. 6). In this work, the narrow band region is denoted by η. The crack is identified first and the level set functions are computed at the grid points in a predetermined region on both sides of crack. In the present work, the half width (r_f) of the narrow band is taken as $1.1d_I$ which is slightly longer than the domain of influence for a regular meshfree node.

Generally, the level set data are stored at the grid points that coincide with the meshfree nodes. Since coarser meshfree nodal discretization is used in this work, significant error can occur

during the activation of level set data at the new grid points [18]. Therefore, a background-refined arrangement of grid points with closer spacing, different from that of meshfree nodes, is used as storage locations. As the crack grows from O to O' (Fig. 7), new grid points are activated. These activated grid points are added to the set p_η.

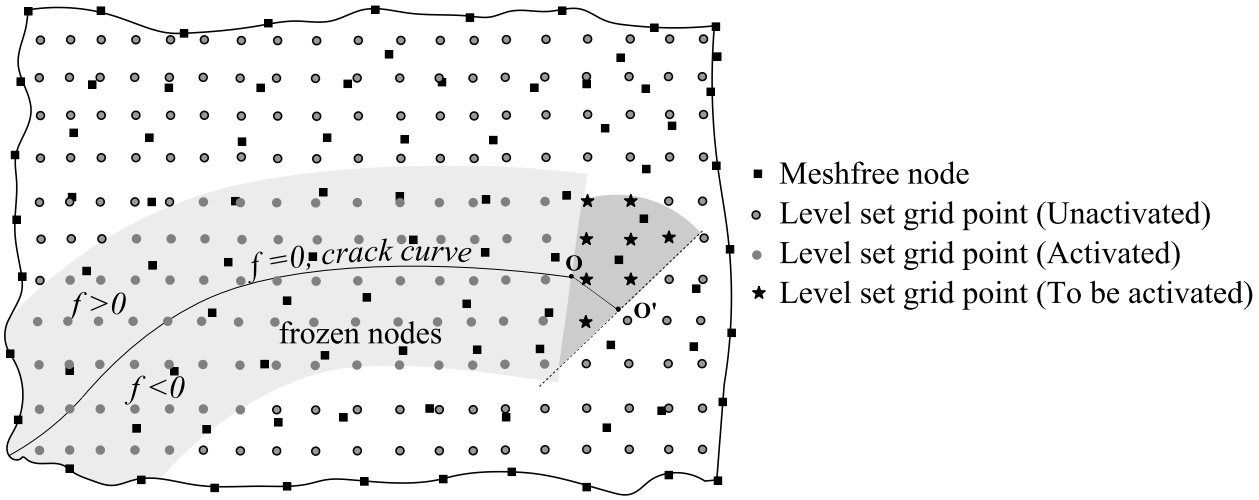

Fig. 7 Meshfree node and level set grid points.

4.1 Level set for a kinking crack

At every grid point, $\mathbf{x}_I$, that lies in the narrow band, a vector level-set function, $\mathbf{f}(\mathbf{x}_I)$, and the sign of the level set function $f(\mathbf{x}_I)$ is stored; for a 2D case, $\mathbf{f}(\mathbf{x}_I) = \Delta x_I \hat{i} + \Delta y_I \hat{j}$ where Δx_I and Δy_I are x and y components of the function $f(\mathbf{x})$. Then, the signed distance function $f(\mathbf{x})$ can be obtained using the relation: $f(\mathbf{x}_I) = \|\mathbf{f}(\mathbf{x}_I)\| H(f(\mathbf{x}_I))$. A compound object $\tilde{f}(\mathbf{x}_I)$ defined as $\tilde{f}(\mathbf{x}_I) = \{\Delta x_I, \Delta y_I, H(f(\mathbf{x}_I))\}^T$ is stored at a grid point that lies inside the narrow band. If there are N grid points in the entire geometry, then the structure of the level set database is given by

$$\tilde{f} = \begin{bmatrix} . & \Delta x_i & . & . & . \\ . & \Delta y_i & . & . & . \\ . & H(f(\mathbf{x}_i)) & . & . & . \end{bmatrix}_{3\times N} \quad i = \{1, 2, ..., N\} \tag{7}$$

Initially all information about level set grid points contains zeroes only. If any grid point is found to lie within the narrow band of a starter crack, then these grid points are activated and the object $\tilde{f}(\mathbf{x})$ is stored at these locations. Let p_η denote the set that consist of grid points inside η, then $\tilde{f}(\mathbf{x}_i) = \{0,0,0\}^T \forall i \notin p_\eta$. Consequently, if any element of the third row of the object $\tilde{f}$ is zero, then the corresponding grid point does not lie in the narrow band region. As the crack extends, the new grid points that fall in the extended narrow band are activated with the level set data $\tilde{f}(\mathbf{x})$, which are easily obtained by some geometric relations for 2D problems [18].

5. LEVEL SET METHOD FOR MULTIPLE NEIGHBOURING CRACKS

Fig. 8 shows the narrow band region for a set of three cracks; 1, 2 and 3. The vector level-set

distance function from a point $\mathbf{x}_I$ that is common to the narrow band of cracks 1 and 2 is shown. The level set object $\tilde{f}(\mathbf{x}_I)$ for a three-crack system can be represented as $\tilde{f}(\mathbf{x}_I) = \left[[\tilde{f}^1(\mathbf{x}_I)] \quad [\tilde{f}^2(\mathbf{x}_I)] \quad [\tilde{f}^3(\mathbf{x}_I)] \right]^T$, where $\tilde{f}^3(\mathbf{x}_I) = \{0,0,0\}^T$ since $\mathbf{x}_I$ does not lie in the narrow band of crack 3. For a set of *n* cracks, the structure is given by

$$\tilde{f} = \begin{bmatrix} [\tilde{f}^1] \\ [\tilde{f}^2] \\ \vdots \\ [\tilde{f}^n] \end{bmatrix}_{3n \times N} \tag{8}$$

Eq. (8) is the extension of Eq.(7) for multiple cracks. This level set structure contains the information about all the cracks in the given geometry through the grid points located in the narrow band region. The narrow band η for a set of *n* cracks is given by $\eta = \eta_1 \cup \eta_2 \cup ... \cup \eta_n$, where η_i is the narrow band region associated with crack i.

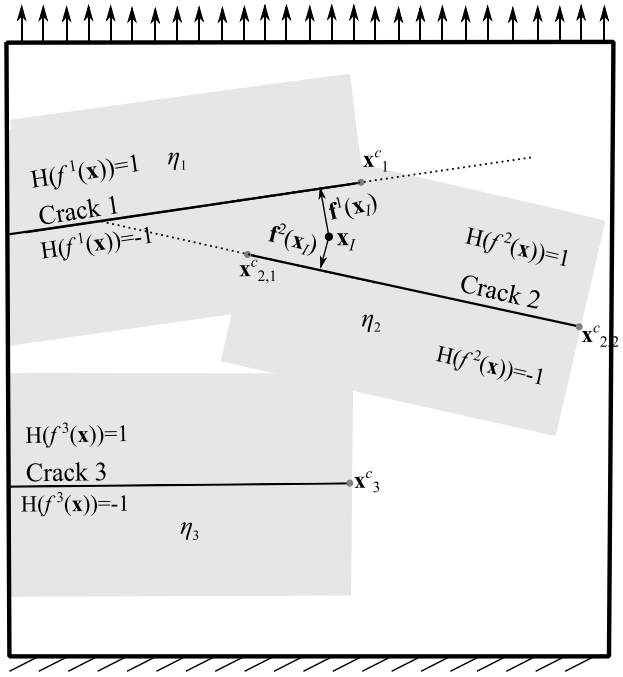

Fig. 8 Level set function for multiple cracks.

5.1 Extrapolating level set function to a generic point

During the evaluation of the global stiffness matrix, it is necessary to determine the sign associated with a generic point such as a Gauss point corresponding to a particular crack. This information is needed for Heaviside enrichment of the nodes that lie in the narrow band. One approach is the use of the closest point projection [18] technique for extrapolation through the vector level-set distance function, $\mathbf{f}(\mathbf{x}_I)$, which is a signed normal vector distance from a point, $\mathbf{x}_I$, to the crack. This technique is implemented by identifying the grid point, $\mathbf{x}_I$, that is closest to the Gauss point, $\mathbf{g}$. Then, $\mathbf{f}(\mathbf{x}_I)$ is extrapolated and the sign at $\mathbf{g}$ can be obtained using

$$\begin{aligned} \mathbf{v}_I &= \mathbf{f}(\mathbf{x}_I) + (\mathbf{x}_I - \mathbf{g}) \\ H(f(\mathbf{g})) &= H(f(\mathbf{x}_I)) \operatorname{sign}\left(\mathbf{f}(\mathbf{x}_I) / \left\| \mathbf{f}(\mathbf{x}_I) \right\| . \mathbf{v}_I \right) \end{aligned} \tag{9}$$

If the level set grid discretization is coarse, or the slope of the current crack advance vector

increases, or the magnitude of the current crack advance vector is small, then the extrapolation according to Eq. (9) will be less precise. To increase the accuracy of the extrapolation, a procedure involving triangular coordinates is used as shown in Fig. 9. This is done by identifying three closest level-set grid points that form a triangle. The triangular or barycentric coordinates of Gauss point $\mathbf{g}$ is found. The signed level-set distance function $f(\mathbf{g})$ can be found using the following relation.

$$f(\mathbf{g}) = L_1 f(\mathbf{x}_1) + L_2 f(\mathbf{x}_2) + L_3 f(\mathbf{x}_3) \tag{10}$$

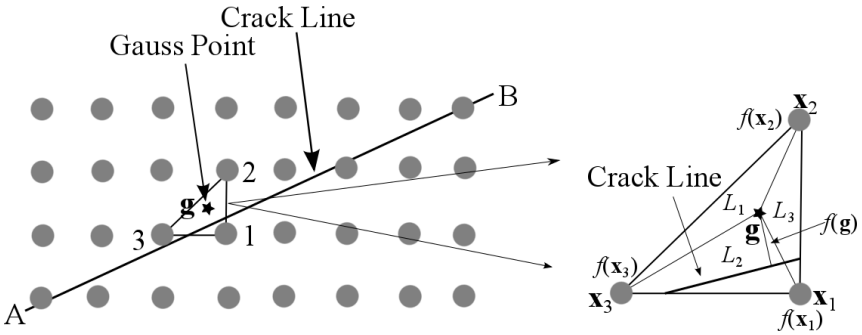

Fig. 9 Extrapolation based on triangular coordinates from level set grid points.

The Heaviside function $H(f(\mathbf{g}))$ at $\mathbf{g}$ is +1 and -1 when $\mathbf{g}$ is above and below the crack respectively. In the absence of three grid points that form a triangle, the 1D extrapolation described in Eq. (9) is used to determine the sign at $\mathbf{g}$. The extrapolation described above can also be used in the case of a curved crack, because the segment of the curved crack lying within the triangle can be approximated by a straight segment.

5.2 Determination of diffracted region

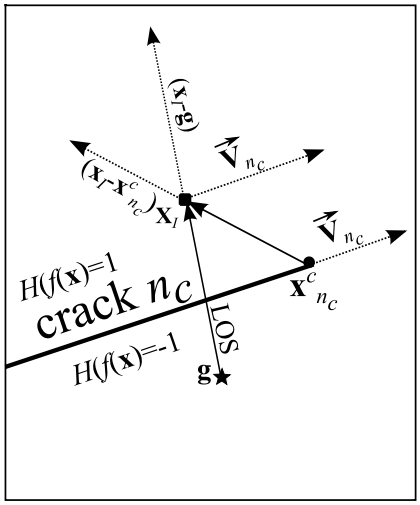

Fig. 10 Barrier crack.

In the diffraction method, a light ray emitted from a source node diffracts around the crack tip and some part of the region behind the crack would form the shadow region. As mentioned in Section 3, the main aspect of this method is to find the shortest distance between the source node and the generic point $\mathbf{g}$ and use this information in Eq. (4) to determine the modified distance. Whether $\mathbf{g}$ falls in the shadow region or not depends upon the position of the crack tip, the source node and the location of $\mathbf{g}$. Let line-of-sight (LOS) be a straight line drawn from a node I located at $\mathbf{x}_I$ to $\mathbf{g}$ (Fig. 10). Any crack extended infinitely, if it intersects the LOS, is considered a potential crack. Let P_c be defined as a set of potential cracks. Whether a crack

labelled n_c is a potential crack or not can be obtained through the following relation based on the sign of the level-set distance function, $f^{n_c}(\mathbf{x})$, corresponding to crack n_c,

$$H(f^{n_c}(\mathbf{x}_I)) \neq H(f^{n_c}(\mathbf{g})) \tag{11}$$

$H(f^{n_c}(\mathbf{x}_I))$ and $H(f^{n_c}(\mathbf{g}))$ can be obtained from Eq. (10). The inequality in Eq. (11) holds true only if node *I* and $\mathbf{g}$ are on the opposite sides of crack n_c.

5.2.1 Shadow region for single edge crack

Only some cracks in the set P_c truly intercept the LOS vector from $(\mathbf{x}_I - \mathbf{g})$ and create a shadow in part of the region around the crack tip. Such cracks are termed as barrier cracks in this work. Barrier cracks are always a subset of potential cracks. For example, in Fig. 10, the potential edge crack labelled n_c is also a barrier crack.

Fig. 11(a) shows the Boolean of Eq. (11), based on the sign of any generic point and sign of source node *I* at $\mathbf{x}_I$ within its d_I. However, the region denoted by A does not actually lie in shadow, as any generic point in A is directly visible to node *I*. Therefore, additional mathematical expressions are needed to identify a barrier in a list of potential cracks.

A potential crack will become a barrier for a particular $(\mathbf{x}_I, \mathbf{g})$ combination if the LOS vector $(\mathbf{x}_I - \mathbf{g})$ lies between the two vectors - the crack front vector $\vec{\mathbf{V}}_{n_c}$ and $(\mathbf{x}_I - \mathbf{x}^c_{n_c})$. This is given mathematically by

$$\begin{aligned} \left[\vec{\mathbf{V}}_{n_c} \times (\mathbf{x}_I - \mathbf{g})\right] \square \left[\vec{\mathbf{V}}_{n_c} \times (\mathbf{x}_I - \mathbf{x}^c_{n_c})\right] > 0 \\ \left[(\mathbf{x}_I - \mathbf{x}^c_{n_c}) \times (\mathbf{x}_I - \mathbf{g})\right] \square \left[(\mathbf{x}_I - \mathbf{x}^c_{n_c}) \times \vec{\mathbf{V}}_{n_c}\right] > 0 \end{aligned} \tag{12}$$

where $\times$ and $\square$ represent the cross and dot product respectively. The first expression implies that the rotational direction from $\vec{\mathbf{V}}_{n_c}$ to $(\mathbf{x}_I - \mathbf{g})$ is the same as from $\vec{\mathbf{V}}_{n_c}$ to $(\mathbf{x}_I - \mathbf{x}^c_{n_c})$. The second expression implies that the rotational direction from $(\mathbf{x}_I - \mathbf{x}^c_{n_c})$ to $(\mathbf{x}_I - \mathbf{g})$ is the same as from $(\mathbf{x}_I - \mathbf{x}^c_{n_c})$ to $\vec{\mathbf{V}}_{n_c}$. Eq. (12) will not be true when $\mathbf{g}$ lies in region A. Both expressions of Eq. (12) are applicable only to identify barrier cracks in a list of potential cracks.

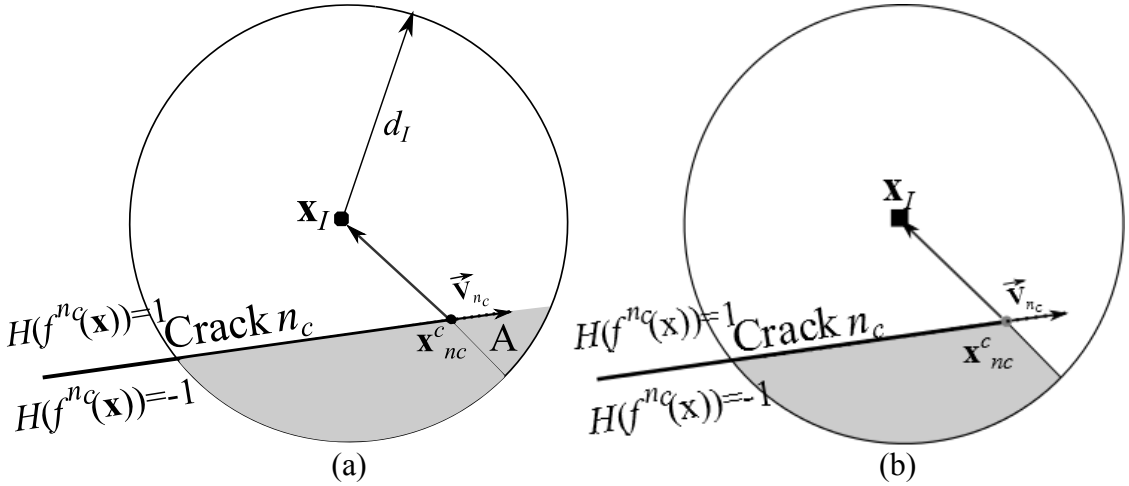

Fig. 11 (a) Boolean of Eq. (11). **(b)** Boolean of Eq. (11) and Eq. (12).

As a result, Eq. (11) and Eq. (12) show the true shadow region as shown in Fig. 11(b). Any point in the darker region is not directly visible to the source node I ; therefore the weight function of node I gets diffracted in this region. In fact, the same conditions can also be used for application of the 'visibility' method of modelling a crack.

If a crack is a barrier crack, then $s_1 = \left(\mathbf{x}_I - \mathbf{x}_{n_c}^c\right)$ and $s_2(\mathbf{g}) = \left(\mathbf{g} - \mathbf{x}_{n_c}^c\right)$; $s_1 + s_2(\mathbf{g})$ is the shortest route from the node I to $\mathbf{g}$. If it is not a barrier crack, then $s_1 + s_2(\mathbf{g}) = s_o(\mathbf{g}) = \left(\mathbf{x}_I - \mathbf{g}\right)$. These values are substituted in Eq. (4) and Eq. (5) to get the profile of the weight function of node I.

5.2.2 Shadow region for two neighbouring cracks

In a multi crack system, when multiple cracks intercept a LOS, the shortest route may have to pass through many barrier crack tips. Such tips are termed as junctions in this work. To determine whether the route passes through a particular tip depends on the location of the source node and/or the previous junctions.

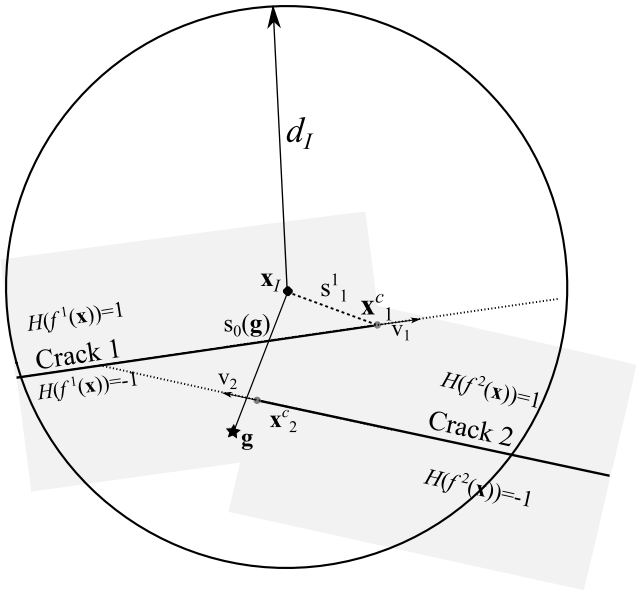

Fig. 12 A two-crack system.

Consider an example of a two-crack system, in which the node I at $\mathbf{x}_I$ has both crack tips, $\mathbf{x}_1^c$ and $\mathbf{x}_2^c$ within its domain of influence with radius d_I (Fig. 12). In the first step, for the $(\mathbf{x}_I, \mathbf{g})$ combination, both cracks, 1 and 2, are potential cracks, but crack 2 is not a barrier crack. The shortest route to $\mathbf{g}$ has to first pass through the crack tip $\mathbf{x}_1^c$, as it is closer to $\mathbf{x}_I$. Consequently, the route kinks at $\mathbf{x}_1^c$ and tries to reach point $\mathbf{g}$. Now, the crack tip $\mathbf{x}_1^c$ becomes the junction i.e. $\mathbf{x}_1^c$ behaves like a proxy source node.

A tip of a particular crack can behave only once as a junction; the shortest route cannot go through any junction more than once. Let L_c be a set consisting of crack labels whose tips behaved as junctions. Initially L_c will be a null set.

Since $\mathbf{x}_1^c$ becomes a junction, crack 1 is added to the set L_c. At this point, the problem is redefined i.e. to find the shortest distance between the junction $\mathbf{x}_1^c$ and $\mathbf{g}$. If a straight line is

drawn from $\mathbf{x}_1^c$ to $\mathbf{g}$, it gets obstructed by crack 2 and the shortest route to $\mathbf{g}$ will kink at $\mathbf{x}_2^c$ which becomes a junction (Fig. 13). As there are no cracks to intercept the LOS i.e. the ray from $\mathbf{x}_2^c$ to $\mathbf{g}$, $s_2(\mathbf{g})$ is computed. Therefore, the shortest route consists of distances s_1^1, s_1^2 and $s_2(\mathbf{g})$. It is to be noted that crack 2 was not a barrier crack initially, but it becomes a barrier for the redefined problem.

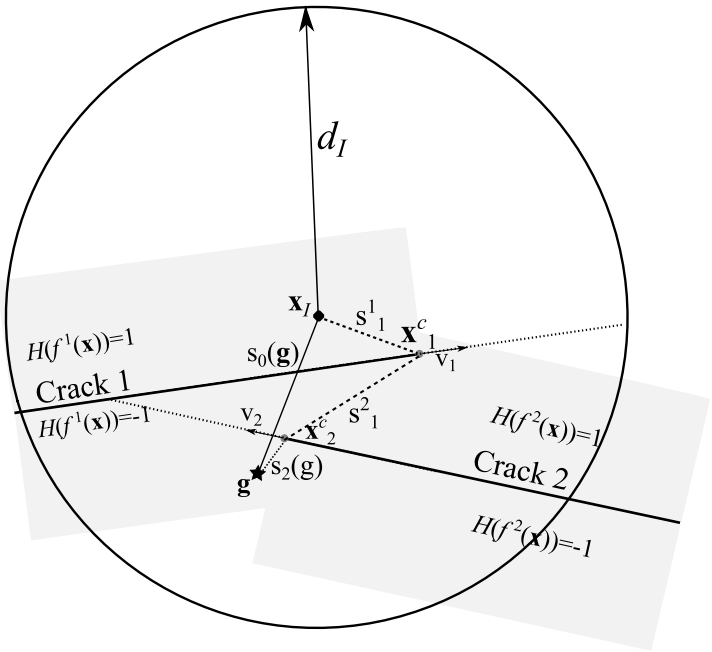

Fig. 13 Determination of shortest route from a crack tip junction.

5.3 Procedure for finding shadow region for multiple cracks

The problem of determining the parameter, $s_1(s_1 = s_1^1 + s_1^2 + \ldots s_1^n)$, continues until there are no more cracks to obstruct the route. This principle to determine the shortest route from a source node to a generic point, in the case of many cracks, remains the same as in the case of double cracks.

General procedure to find the diffracted region

1. Determine the family of potential cracks P_c such that $P_c \cap L_c = \varnothing$.
2. Sort the P_c, in ascending order, based on the proximity of the node ($\mathbf{x}_I$) to the crack tips.
3. Loop through all the cracks in the sorted P_c.
   a. If a crack labeled n_c is a barrier crack, then obtain the new proxy node $\mathbf{x}_{n_c}^c$ and compute s_1^n - (n here being the iteration number).
   b. Exit the loop when P_c is a null set or have run through all the cracks in P_c. Else, go back to step 1.
4. Calculate $s_2(\mathbf{g})$ in the end.

Example - A five crack system

To illustrate this procedure, a five-crack arrangement with the location of source node $\mathbf{x}_I$ and Gauss point $\mathbf{g}$ is shown in Fig. 14(a). In the first iteration, a LOS is obstructed by crack 1, 4 and 5. Since crack 1 is the closest, the route gets kinked at $\mathbf{x}_1^c$, which becomes the new junction for the next iteration (Fig. 14(b)). In the second iteration, the LOS from $\mathbf{x}_1^c$ to $\mathbf{g}$ is obstructed

first by crack 3; crack 2 does not interrupt LOS. So, the route gets kinked again at the tip $\mathbf{x}_3^c$ (Fig. 14(c)). In the third iteration, the LOS from $\mathbf{x}_3^c$ to $\mathbf{g}$ gets obstructed by crack 5. Therefore, the route gets kinked at the tip $\mathbf{x}_5^c$ and finally there is no obstruction for the LOS from $\mathbf{x}_5^c$ to $\mathbf{g}$ (Fig. 14(d)).

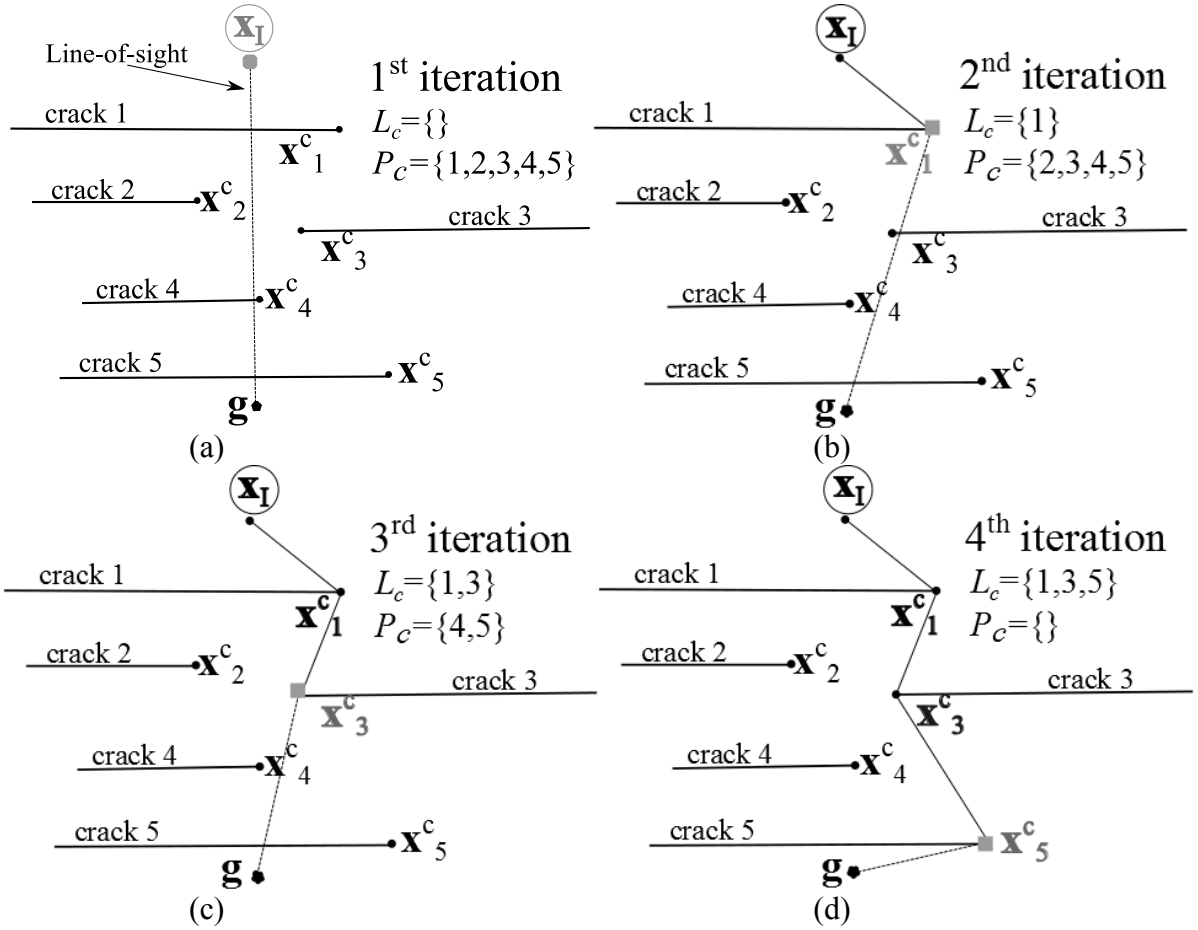

Fig. 14 Shortest distance between node and a sampling point **(a)** Iteration 1 **(b)** Iteration 2 **(c)** Iteration 3 **(d)** Iteration 4.

5.4 Examples of shadow regions arising from multiple crack arrangements

Fig. 15(a) and Fig. 15(b) show the diffracted region and the weight functions of a node $\mathbf{x}_I$ in the presence of two parallel cracks. The grey and black asterisk markers indicate the region with non-zero and zero weight function, respectively. The zero weight-function regions correspond to the shadow region cast by the crack. The weight function gets truncated near the crack tip regions of the cracks as shown in Fig. 15(b). The procedure Section 5.3 requires that no source node contain both crack tips of a single crack in its domain of influence.

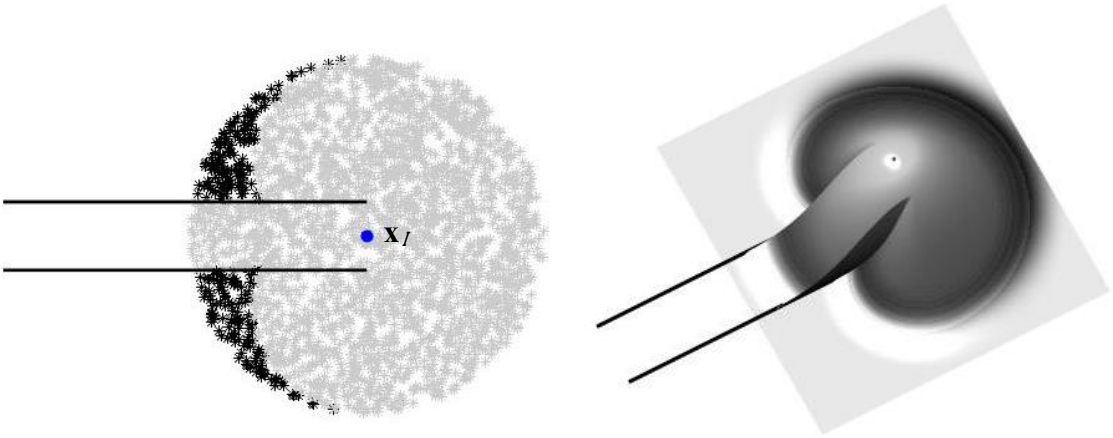

(a) (b)

Fig. 15 Diffracted region in **(a)** an arrangement of two parallel cracks. **(b)** truncated weight function of the node $\mathbf{x}_I$.

In the second case (Fig. 16(a)), the source node $\mathbf{x}_I$ is located just below crack 1. Therefore, the region below crack 1 has a non-zero value of the weight function. The region above crack 1 close to its tip also has a non-zero weight function due to diffraction. The weight function gets truncated because of the diffraction method, in the presence of crack tips that act as sharp corners (Fig. 16(b)).

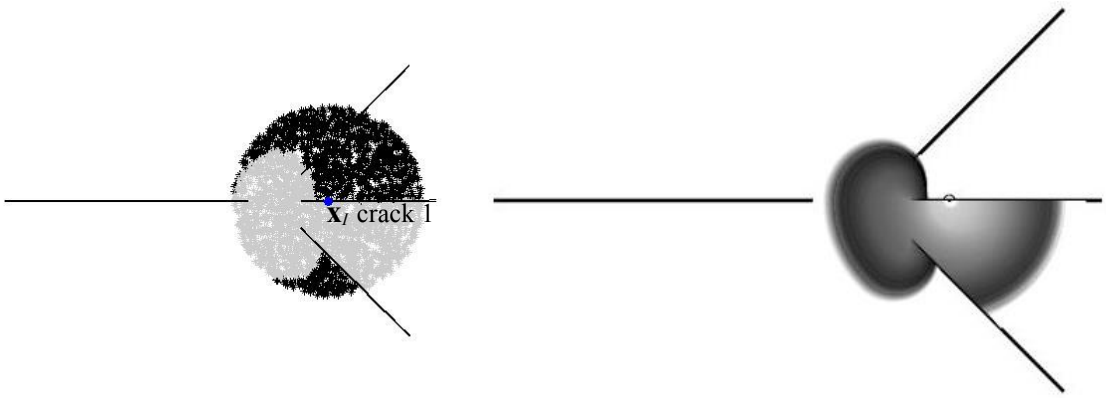

(a) (b)

Fig. 16 Diffracted region in **(a)** an arrangement of four cracks. **(b)** truncated weight function of the node $\mathbf{x}_I$.

To illustrate further for a hypothetical case, a case of multiple cracks, in close proximity, with the diffracted regions, is shown in Fig. 17.

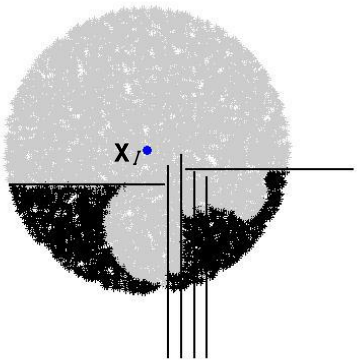

Fig. 17 Diffracted region in an arrangement of multiple cracks.

5.5 Shadow region for a kinking crack

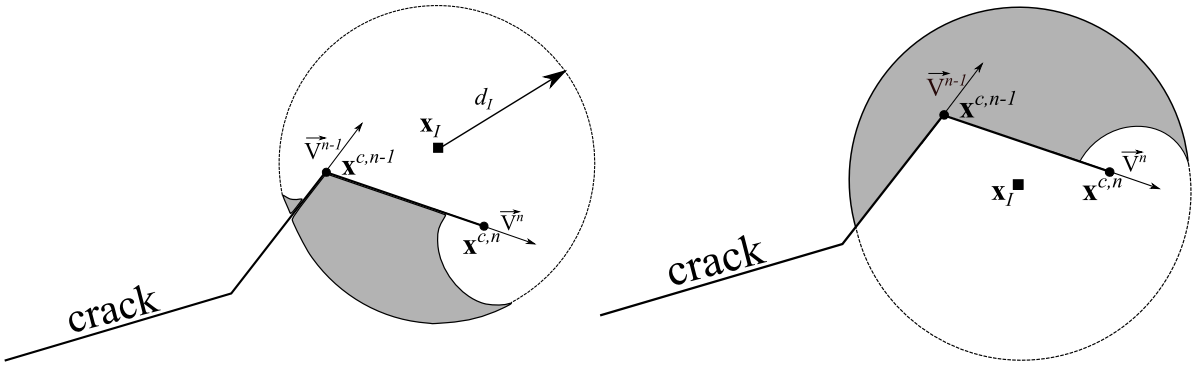

Fig. 18 Diffraction in case of kinked crack.

Eq. (12) is not applicable for kinked cracks because a kink location (Fig. 18(a) and (b)) can affect the LOS. In other words, the kinks of the same crack come up as a barrier for the LOS. In order to determine the shortest route, it is also necessary to check whether the LOS from a source node or a kink point, including a crack tip such as $\mathbf{x}^{c,k}$ $\left(k=\{0,1,2,...,n\}\right)$ to a generic point, is obstructed by segments between two kinks.

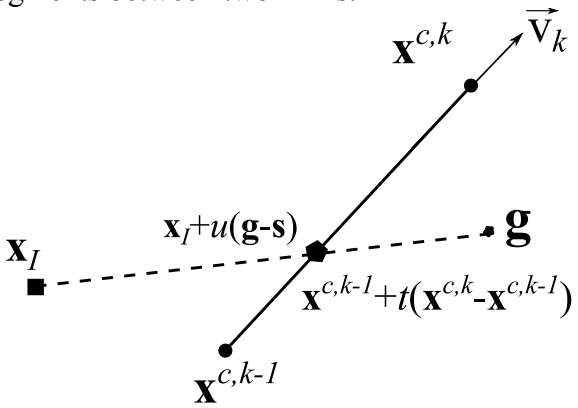

Fig. 19 Intersection of two line segments.

We define the k^{th} kink vector $\vec{\mathbf{V}}_k=\mathbf{x}^{c,k}-\mathbf{x}^{c,k-1}$ and express the k^{th} kink segment in the parametric form as $\mathbf{x}^{c,k-1}+t(\mathbf{x}^{c,k}-\mathbf{x}^{c,k-1})$, where t $(0\le t\le 1)$ is a scalar parameter. Similarly, the LOS can also be expressed in the parametric form as $\mathbf{s}+u(\mathbf{g}-\mathbf{s})$, where $\mathbf{s}$ can be a source node or kink points and u $(0\le u\le 1)$ is a scalar parameter. In order to find the intersection point of k^{th} kink segment and the LOS, we set $\mathbf{x}^{c,k-1}+t(\mathbf{x}^{c,k}-\mathbf{x}^{c,k-1})=\mathbf{s}+u(\mathbf{g}-\mathbf{s})$ (Fig. 19) and solve t and u values. The parameters t and u can be expressed as

$$
\begin{aligned}
t &= \left(\mathbf{x}_I-\mathbf{x}^{c,k-1}\right)\times(\mathbf{g}-\mathbf{s})\Big/\left((\mathbf{g}-\mathbf{s})\times\left(\mathbf{x}^{c,k}-\mathbf{x}^{c,k-1}\right)\right)\\
u &= \left(\mathbf{x}_I-\mathbf{x}^{c,k-1}\right)\times\left(\mathbf{x}^{c,k}-\mathbf{x}^{c,k-1}\right)\Big/\left((\mathbf{g}-\mathbf{s})\times\left(\mathbf{x}^{c,k}-\mathbf{x}^{c,k-1}\right)\right)
\end{aligned}
\qquad (13)
$$

Whether the kink vector $\vec{\mathbf{V}}_k$ actually intersects can be found by the condition $0\le t\le 1$ and $0\le u\le 1$ of Eq. (13).

Fig. 20 shows an example of a multiple kinking crack. The LOS from $\mathbf{x}_I$ to $\mathbf{g}$ is intercepted

by the kink segments $\vec{V}_{n-1}$ and $\vec{V}_{n-2}$ meeting at $\mathbf{x}^{c,n-2}$. Geometrically, this means that the kink $\mathbf{x}^{c,n-2}$ is located below the LOS and the sign of $\mathbf{g}$ i.e. $H(f^1(\mathbf{g}))$ is -ve for the kink $\mathbf{x}^{c,n-2}$ to behave as a junction.

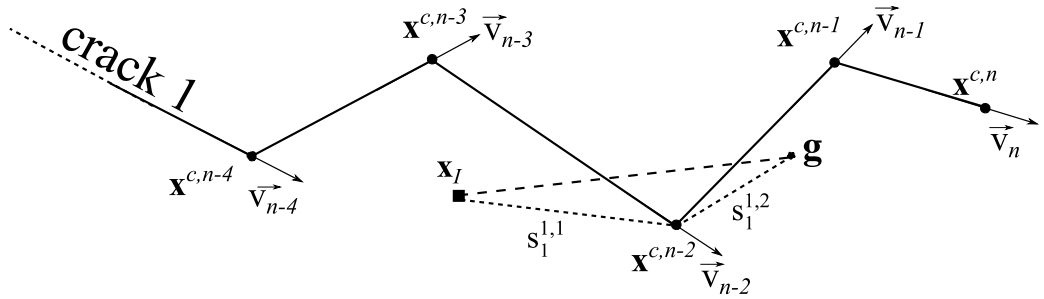

Fig. 20 Step-by-step crack propagation; $\mathbf{g}$ is below the crack.

Consider Fig. 21, where the sign of $\mathbf{g}$ is +ve, i.e. $\mathbf{g}$ lies above the crack. The kink segments $\vec{V}_{n-2}$ and $\vec{V}_{n-3}$ intersect the LOS. $\mathbf{x}^{c,n-3}$ is located above the LOS, and therefore behaves as a junction.

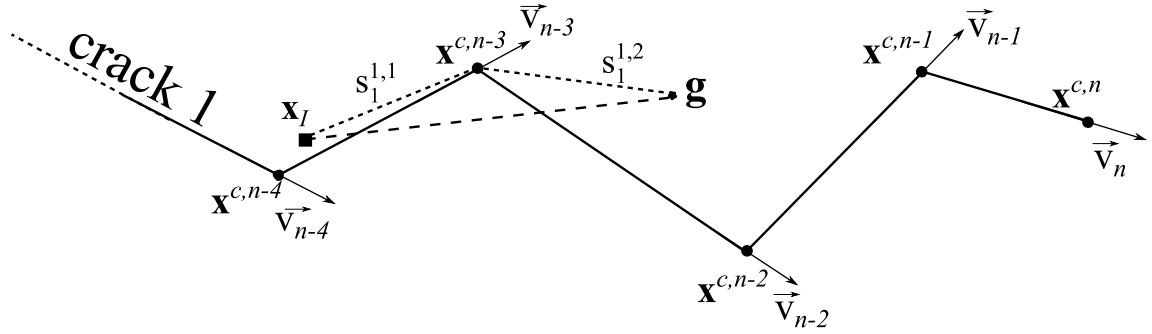

Fig. 21 Step-by-step crack propagation; $\mathbf{g}$ is above the crack.

In both the above-mentioned cases, the shortest route becomes $s_1 = s_1^{1,1} + s_1^{1,2}$. The positioning of kink location $\mathbf{x}^{c,k}$ $\left(k = \{0,1,2,...,n\}\right)$ with respect to the LOS and the sign of $\mathbf{g}$ with respect to the crack, will determine if $\mathbf{x}^{c,k}$ can act as a junction.

In the case of multiple kinks within the domain of influence (radius d_I) of node at $\mathbf{x}_I$, a particular kink location $\mathbf{x}^{c,k}$ $\left(k = \{0,1,2,...,n\}\right)$ acts as a junction only if it satisfies $0 \le t \le 1$ and $0 \le u \le 1$ (Eq. (13)) and the following condition.

$$H(\ell(\mathbf{x}^{c,k})) = H(f^{n_c}(\mathbf{g})) \tag{14}$$

where ℓ is the equation of the LOS given by the form $y\text{-}mx\text{-}b = 0$; m is the slope and b is the y-intercept.

For kinked cracks, the general procedure described in Section 5.3 is modified by taking into account the intra-crack barriers due to kinks. Based on this, the diffracted region for a single and double kinked crack is shown in Fig. 22(a) and Fig. 22 (b) respectively.

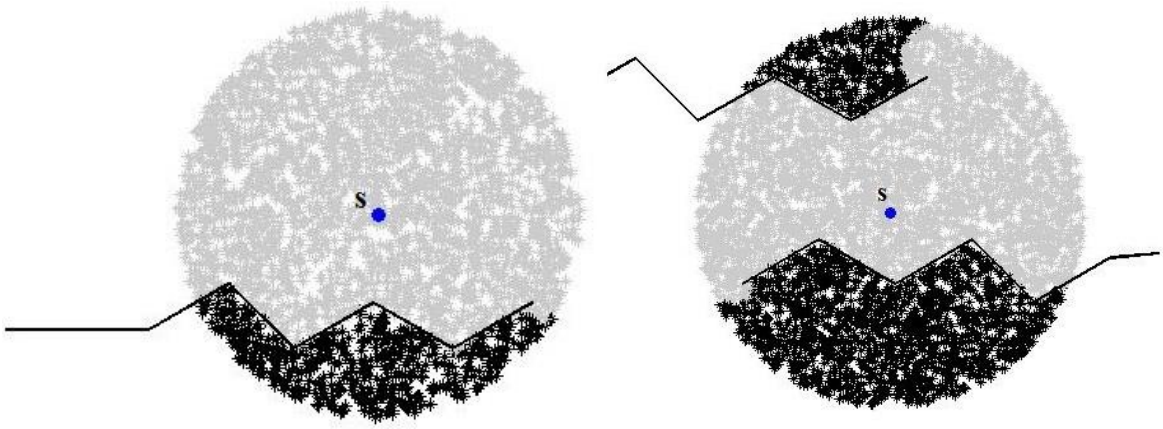

(a) (b)

Fig. 22 Diffraction region in case of **(a)** single crack. **(b)** double crack.

In the case of a kinking crack, there is also a knee singularity at the kink in addition to the crack tip singularity. In order to capture this interaction effect, the diffraction node's influence is restricted to two kink locations. The procedure described in this section may also be used for straight cracks, but is computationally cumbersome in comparison to the approach described in Section 5.3.

6. INTERACTION INTEGRAL TO EXTRACT SIFs

In the present work, mixed mode SIFs are computed through the popular interaction integral/M-integral [37]. For a crack in a homogenous material in absence of thermal load and crack face loading, the interaction integral is given by

$$I = \int_A (\sigma_{ij} u_{i,1}^{aux} + \sigma_{ij}^{aux} u_{i,1} - \sigma_{ik} \varepsilon_{ik}^{aux} \delta_{1j}) q_{,j} dA \tag{15}$$

where A is the area of integration as shown in Fig. 23(a). q is a scalar function which has a value of unity on the contour S_1 and zero on S_2. δ_{ij} is the Kronecker's delta. The integration is carried out by shrinking the area A_o to zero. σ_{ij}^{aux}, ε_{ik}^{aux} and u_i^{aux} are auxiliary state values that correspond to the theoretical crack tip solution in a homogenous material.

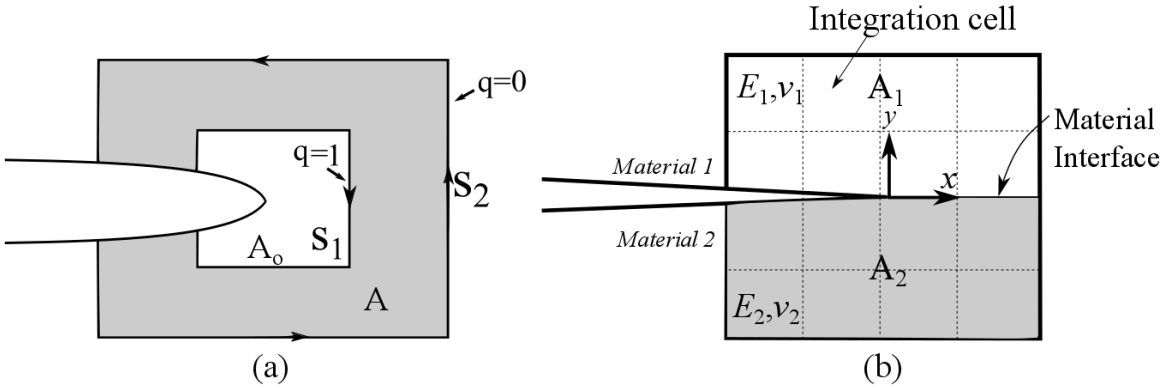

(a) (b)

Fig. 23. (a) Area for domain integral. **(b)** Domain of integration for interface crack.

For a crack in an isotropic and homogenous material, interaction integral/M-integral is equal to

$$I = \frac{(2K_I K_I^{aux} + 2K_{II} K_{II}^{aux})}{E^*} \tag{16}$$

where E^* is E for plane stress and $E/(1\text{-}v^2)$ for plane strain. E and v are Young's modulus and Poisson's ratio respectively. K_I is evaluated by setting K_I^{aux} to unity and K_{II}^{aux} to zero. Similarly K_{II} is evaluated by setting K_{II}^{aux} to unity and K_I^{aux} to zero.

In case of interface crack in bi-materials as shown in Fig. 23(b), subjected to mechanical load, the interaction integral is given by

$$I = \sum_{m=1}^{2} \int_{A_m} (\sigma_{ij} u_{i,1}^{aux} + \sigma_{ij}^{aux} u_{i,1} - \sigma_{ik} \varepsilon_{ik}^{aux} \delta_{1j}) q_{,j} dA \tag{17}$$

$\sigma_{ij}^{aux}, \varepsilon_{ik}^{aux}$ and u_i^{aux} are crack tip solution for auxiliary state with an interface crack [38]. The SIFs can be computed using the following relation.

$$I = \frac{(1/E_1^* + 1/E_2^*)(2K_I K_I^{aux} + 2K_{II} K_{II}^{aux})}{2\cosh^2(\pi\varepsilon)} \tag{18}$$

ε is given by

$$\varepsilon = \frac{1}{2\pi} \ln\left(\frac{1-\beta}{1+\beta}\right) = \frac{1}{2\pi} \ln\left(\frac{\kappa_1 \mu_2 + \mu_1}{\kappa_2 \mu_1 + \mu_2}\right) \tag{19}$$

where μ_m is the shear modulus and κ_m is the Poisson's ratio, m = 1 and 2. β is one of the Dundurs' parameters. The energy release rate for the interface crack is related to the complex SIF by

$$G = \frac{1}{E^*} \frac{K_1^2 + K_2^2}{\cosh^2(\pi\varepsilon)} \tag{20}$$
$$1/E^* = 1/E_1^* + 1/E_2^*$$

7. CASE STUDIES

The modified EFG method has been applied to a number of problems involving interacting cracks. The nodal domain of influence (radius d_I) is set to 1.75 times the regular nodal spacing. The SIFs are obtained using the interaction integral technique, in all the case studies reported in this section, and the results are compared with those in the literature.

7.1 Double edge cracks

Fig. 24(a) shows a finite plate with double-edge collinear cracks. The plate is subjected to tensile traction of 1MPa. A state of plane strain is assumed. The SIFs are calculated for two plate geometries $L/w = 1$ and $L/w = 3$ with crack length-to-width ratio of $a/w = 0.8$ and $a/w = 0.9$. The computed mode I (K_I) and mode II (K_{II}) SIFs are normalized by $\sigma\sqrt{\pi a}$: $\hat{K}_I = K_I/(\sigma\sqrt{\pi a}), \hat{K}_{II} = K_{II}/(\sigma\sqrt{\pi a})$. Unless specified otherwise, the materials are assumed to be isotropic with Young's modulus $E = 210 GPa$ and Poisson's ratio $v = 0.3$.

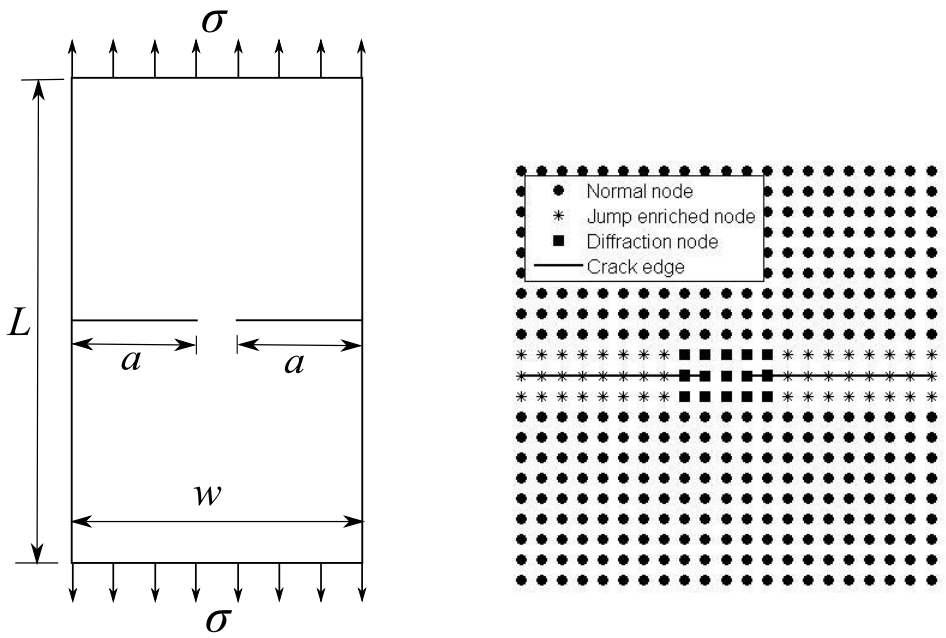

Fig. 24 (a) Double-edge collinear cracks. (b) Nodal Discretization.

Regular nodal discretizations of 21×21 (Fig. 24(b)) nodes for $L/w=1$ and 21×61 nodes for $L/w=3$ are used. This is similar to the nodal discretization used by Muravin *et al.* [25]. However, the bandwidth of the resulting stiffness matrix in the present case is lower than the latter due to a lower value of d_I. The proposed method does not require a higher value of d_I due to the utilization of Heaviside enrichment functions to model the discontinuity of the displacement across the crack edges. The jump enriched nodes are enriched with Heaviside functions. The weight functions of the diffracted nodes get truncated due to the presence of cracks. However, the classical EFG method, where only visibility or diffraction method is used, needs extra nodes along the crack edges or higher value of d_I to avoid an ill-conditioned stiffness matrix.

The normalized mode I SIF ($\hat{K}_I$) is compared with the results obtained by [25] and the analytical solutions of Bowie [39]. The error is computed based on the results of Muravin & Turkel [25]. The comparison in Table 1 shows that there is an excellent agreement though coarser nodal discretization and low d_I was employed in the present study.

Table 1 Comparison of normalized SIF for double-edge cracks.

a/w	L/w	$\hat{K}_I$ [25]	$\hat{K}_I$ [39]	$\hat{K}_I$ Present Method	% Error*
0.8	1	1.6111	1.5806	1.6085	-0.161 %
0.8	3	1.5497	1.5649	1.5454	-0.278 %
0.9	1	2.1326	2.1133	2.1231	-0.446 %
0.9	3	2.1016	2.1133	2.0993	-0.109 %

* % error is with respect to Muravin and Turkel (2006) results.

7.2 Four neighbouring cracks

In this example (Fig. 25(a)), a finite plate has four cracks whose crack tips lie in close proximity. The plate is subjected to a tensile load of 1MPa. A state of plane strain is assumed. The SIFs are calculated for $L=4$ and crack length-to-width ratio $a/w=0.45$. There is a strong

interaction among the four crack-tip singular stress fields. In order to capture such a complex field accurately, the classical EFG needs a fine nodal discretization in the region encompassing the crack tips. However, the MCW function reduces the complexities involved.

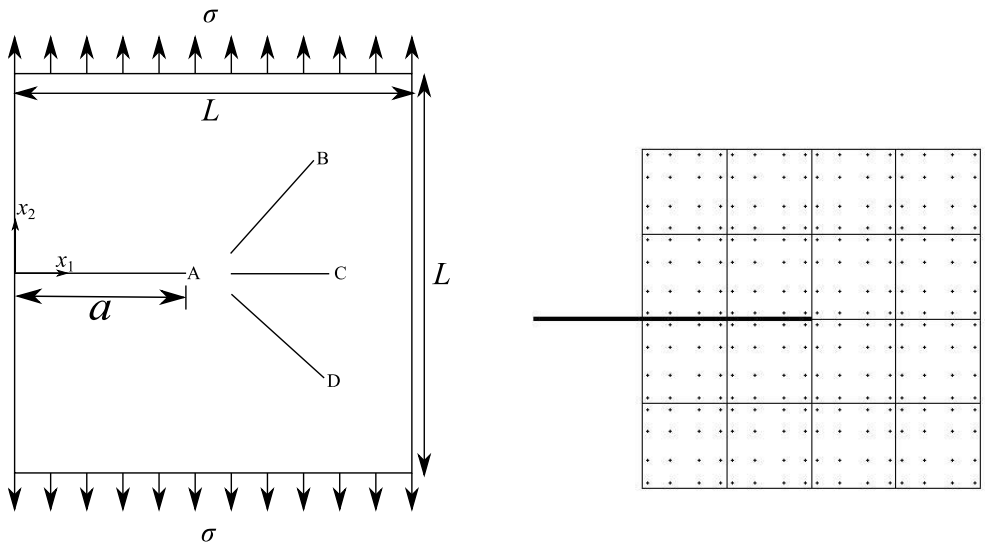

(a) (b)

Fig. 25 (a) Finite plate with four cracks under uniform tensile loading. (b) Interaction integral domain with Gauss points.

The end coordinates of cracks B, C and D are (2.2,0.2), (3,1); (2.2,0), (3.2,0); and (2.2,-0.2), (3,-1) respectively. The singular stress field at the tip of edge crack A interacts strongly with the neighbouring crack-tip stress fields of crack B, C and D. The SIFs are obtained using the interaction integral whose integral domain is a square of edge length $0.2a$. The distribution of Gauss points for numerical integration is indicated by the dots shown in Fig. 25(b).

Table 2 shows a comparison of the computed normalized mode I SIFs at the tip of crack A with the published data by Muravin & Turkel [25] for three nodal discretizations. It is to be noted that satisfactory results are obtained even with a very coarse nodal density and low d_I.

Table 2 Comparison of normalized SIFs for edge crack interacting with three neighbouring cracks.

Nodal Discretization	$\hat{K}_I$ [25]	$\hat{K}_I$ Present Method	% Error
21×21	2.80114	2.7789	-0.793 %
41×41		2.7963	-0.171 %
81×81		2.8020	0.032 %

7.3 Cross cracks and star cracks

Fig. 26(a) and Fig. 26(b) show cross cracks and star cracks in a square plate of width $w = 4$ units subjected to bi-axial loads. The normalized mode I SIFs are obtained for various a/w ratios. In order to increase the accuracy and capture the singular field accurately in this case, the region around the crack tip is slightly refined. This process is not cumbersome as in the case of mesh-based methods. Further, the usage of a Heaviside function to model a crack reduces the need to add any extra nodes along the crack, like in the case of pure diffraction based approach.

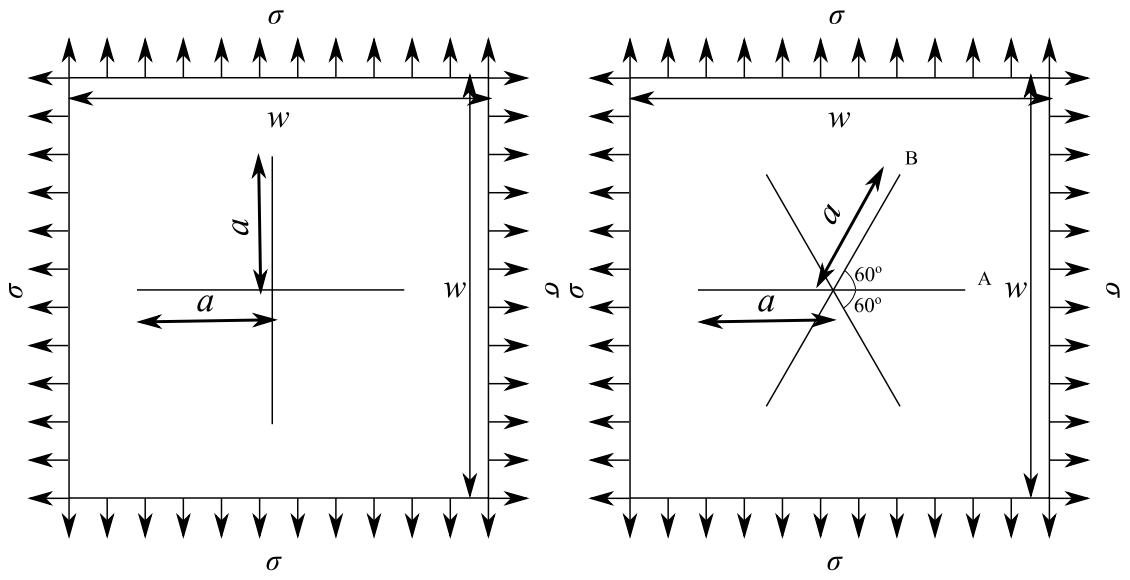

Fig. 26 (a) Cross cracks. **(b)** Star cracks.

Table 3 Comparison of normalized SIFs for cross cracks in square plate.

a/w	$\hat{K}_I$ [40]	$\hat{K}_I$ [24]	$\hat{K}_I$ Present Method	% error*
0.1	0.8641	0.8655	0.8563	-1.059 %
0.2	0.8800	0.8837	0.8837	0.000 %
0.3	0.9092	0.9126	0.9132	0.060 %
0.4	0.9537	0.9670	0.9583	-0.901 %
0.5	1.0223	1.0370	1.0273	-0.938 %
0.6	1.1300	1.1450	1.1361	-0.781 %
0.7	1.2866	1.3300	1.3182	-0.884 %
0.8	1.4857	1.6500	1.6550	0.300 %
0.9	-	2.4400	2.4650	1.025 %

* % error is with respect to the results of Barbieri et al. [24]

Table 3 shows a comparison of the computed normalized mode I SIF ($\hat{K}_I$) for the case of cross cracks. The present results are in good agreement with the results obtained by an enriched meshfree method based on the reproducing kernel particle method (RKPM) [24].

Fig. 27 shows a comparison of the normalized SIFs for a star crack with the results obtained using the EFG method [25] and XFEM [41]. $\hat{K}_I^A \left(K_I^A / \sigma\sqrt{\pi a} \right)$ denotes the normalized mode I SIF for crack tip A. $\hat{K}_I^B \left(K_I^B / \sigma\sqrt{\pi a} \right)$ and $\hat{K}_{II}^B \left(K_{II}^B / \sigma\sqrt{\pi a} \right)$ denote the normalized mode I and mode II SIFs for crack tip B. The comparison shows that the obtained SIFs are in good agreement with the published numerical results.

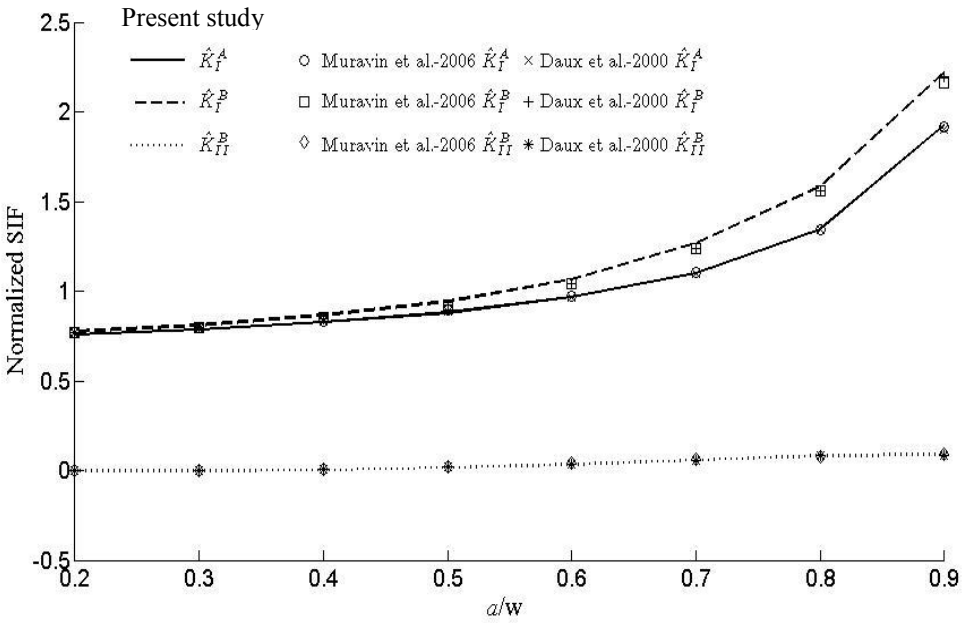

Fig. 27 Variation of normalized SIFs for star crack with a/w .

7.4 Crack-microcrack interaction

Fig. 28(a) shows two stacked microcracks interacting with a macro edge crack in a plate under uniform tensile load. The results are obtained for various h/l ratios. Only the semi-stack height (h) is varied. The geometric specifications are: $w=20\text{mm}$, $L/w=5$, $a/w=0.5$ and $2l/a=0.05$.

The region encompassing the microcracks is refined (Fig. 28(b)) to increase the accuracy of the normalized SIF (K_I/K_{I0}), where K_{I0} is the mode I SIF of the macro crack without the microcracks.

Fig. 29 shows that the obtained SIF agrees satisfactorily with the exiting results in the literature [42,8]. There is a shielding effect at the macrocrack tip when the distance between the macrocrack and the microcracks are small. The shielding effect decreases with the increase in h/l ratio and vanishes beyond the distance of $3.5h/l$.

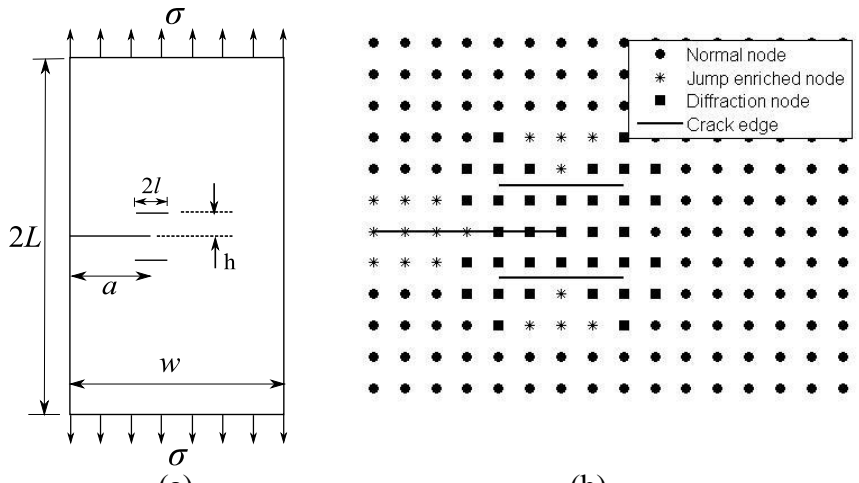

(a) (b)

Fig. 28 (a) Single edge crack with two stacked microcracks (microcrack length not to scale).**(b)** Nodal discretization.

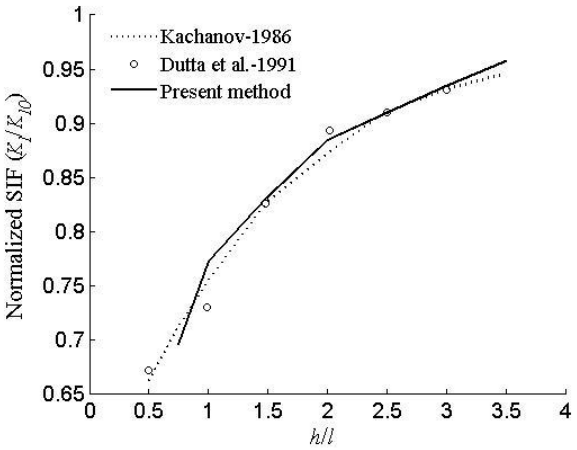

Fig. 29 Comparison of variation of normalized mode I SIF with h/l ratio.

7.5 Interface crack-subinterface crack interaction

Fig. 30(a) shows an interface crack interacting with a subinterface crack in a bi-material plate subjected to uniform tensile load. The geometric specifications of the plate are: $w = 150\,\text{mm}$, $L/w = 4/3$, $a/w = 2/15$, $c/a = 0.2$ and $h = 1.27\,\text{mm}$. The material properties of the ceramic-metal bi-material plate correspond to S45C steel ($E_1 = 206\,\text{GPa}$, $v_1 = 0.3$) and Si_3N_4 ($E_2 = 304\,\text{GPa}$, $v_2 = 0.27$). For analysis, plane stress conditions are assumed in this case.

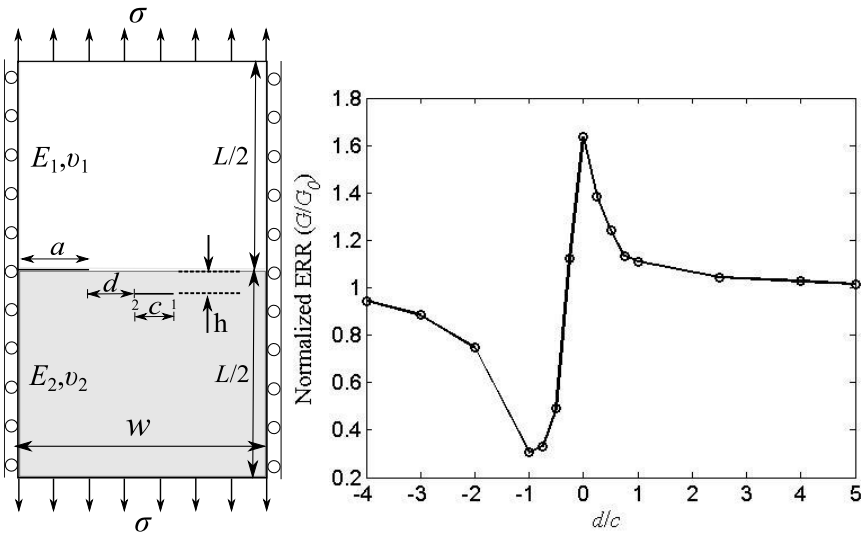

(a) (b)

Fig. 30 (a) Bimaterial plate with interface crack and a subinterface crack under tensile loading. **(b)** Normalized ERR variation with d/c ratio.

The complex SIF ($K_1 + iK_2$) associated with the interface crack is obtained using the interaction integral [38].

Fig. 30(b) shows the variation of the normalized energy release rate (ERR) G/G_0 with d/c ratio. G_0 is the ERR of the interface crack in the absence of a subinterface crack. As the subinterface crack approaches the interface crack tip from the left, the shielding effect is observed. G/G_0 reaches a minimum when the crack tip 1 is close to the interface crack tip. The ratio G/G_0 amplifies rapidly as d/c increases and reaches a maximum when the crack tip 2 coincides with the interface crack tip. Then, it decreases and approaches to unity after $d/c > 4$.

The effect of shielding or amplification is experienced by the interface crack even when the subinterface crack is at distances h, which is several times its length l. Similar trends were also observed by Ouinas et al. [43].

7.6 Double and triple kinked cracks

Fig. 31(a) and Fig. 31(b) show double and triple kinked cracks in rectangular plates under tension. These kinds of zigzag cracks may develop due to stress corrosion cracking. They can also be due to the extension of a mixed mode crack. It involves the interaction of knee point singular fields with the crack tip singular field. In the first case (Fig. 31 (a)), the first kink OA makes an angle of $\theta_1 = 45^o$ with the x_1-axis. The second kink, AB, makes an angle of θ_2 with OA.

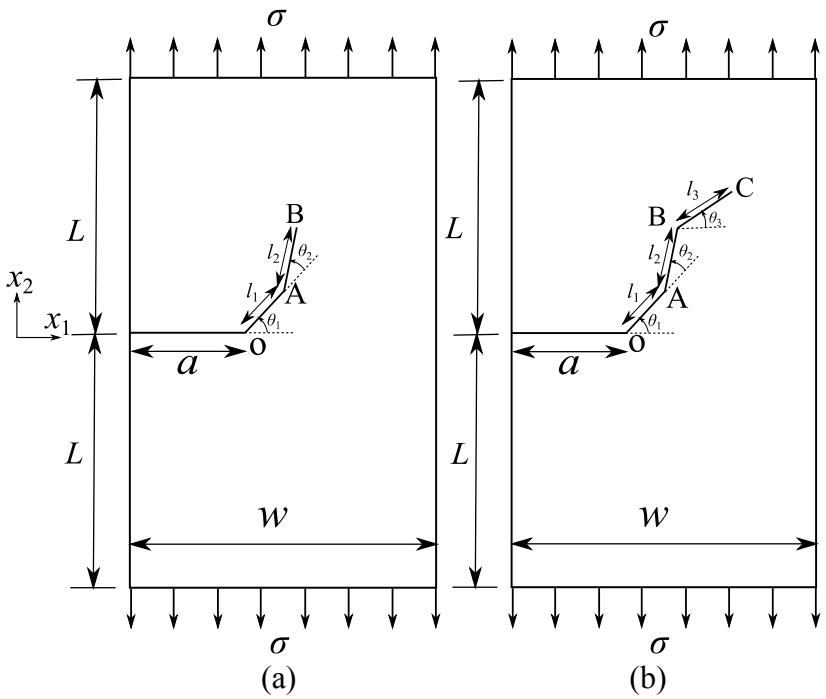

Fig. 31 (a) Double kinked cracks. **(b)** Triple kinked cracks.
$a = 1\text{mm}$, $a/w = 0.5$, $L/w = 2$ and $l_1 = l_2 = l_3 = 0.04a$.

Fig. 32(a) and Fig. 32(b) shows the variation of normalized mode I $\left(K_I / \sigma\sqrt{\pi a}\right)$ and mode II SIFs $\left(K_{II} / \sigma\sqrt{\pi a}\right)$ respectively with θ_2 obtained using nodal discretization strategies such that the diffraction nodes affect one kink and two kinks locations. An example of a case when a diffracted node affects a single kink in a propagating crack is shown in Fig. 18. In such a case, its weight function gets truncated at the two sharp corners: crack tip and the kink. When the diffracted node affects two kinks, then its weight function gets truncated at three sharp corners: crack tip and two kink locations.

The results obtained by both the strategies are in agreement with each other except at the extremities of the plot. This may be due to the interaction of the kink singularity field with the crack tip singularity field.

The normalized mode I SIF reaches its maximum at $\theta_2 = -45^o$ where the mode II SIF is zero. This agrees with the maximum tangential stress (MTPS) criterion [44,45] which dictates that a crack will propagate in the direction of zero shear stress or $K_{II} = 0$.

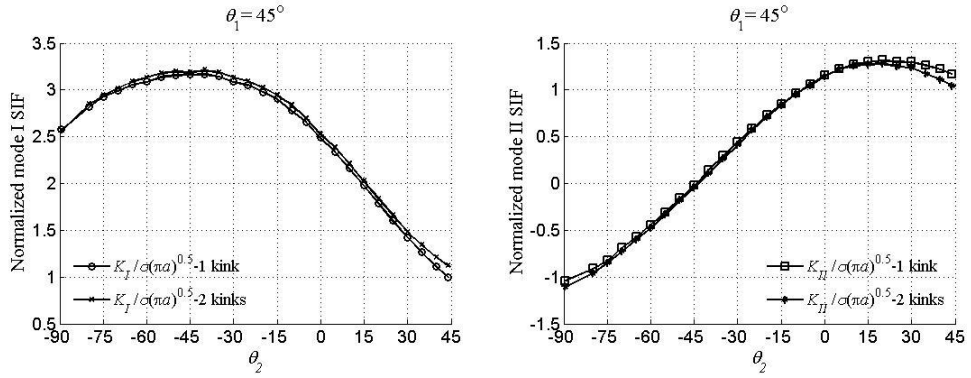

Fig. 32 For for double kinked crack with θ_2 **(a)** Normalized mode I **(b)** Normalized mode II SIF.

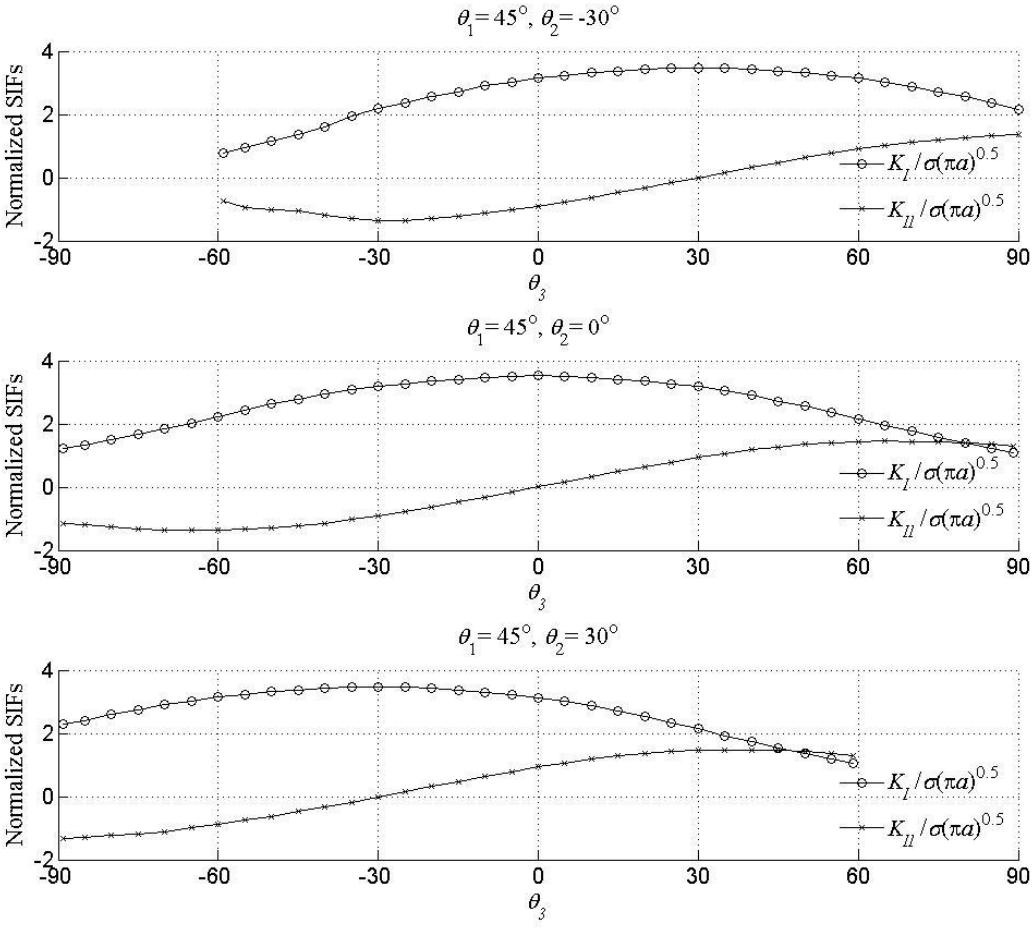

Fig. 33 Variation of normalized mode I and mode II SIFs for triple kinked crack problem with θ_3.

Fig. 33 shows the variation of normalized mode I and mode II SIFs at crack tip C with θ_3 for three values of θ_2. It is observed from each subplot that the maximum value of mode I occurs when $K_{II} = 0$ at the tip C. This is the angle in which the crack is likely to propagate further.

7.7 Multiple crack propagation

Fig. 34 shows a plate subjected to uniform end displacement at the top edge. The plate has two

holes and two cracks. The material properties are E=2×10^5 N/mm^2 and $\nu = 0.3$. This problem has been previously studied using FEM [45,46] and XFEM [47]. In the present study, the holes are modelled using level set enrichment. The MTPS criterion is used to determine the angle of crack propagation. The crack extension length, or kink length, is set to 0.5mm. Two sets of nodal configuration are used: 40×20 and 32×16 with refinement at the crack tip using 9×9 nodes such that diffraction node influences at least one kink point. The level set grid point distribution is 640x320. However, a narrow band centering crack is only activated for analysis.

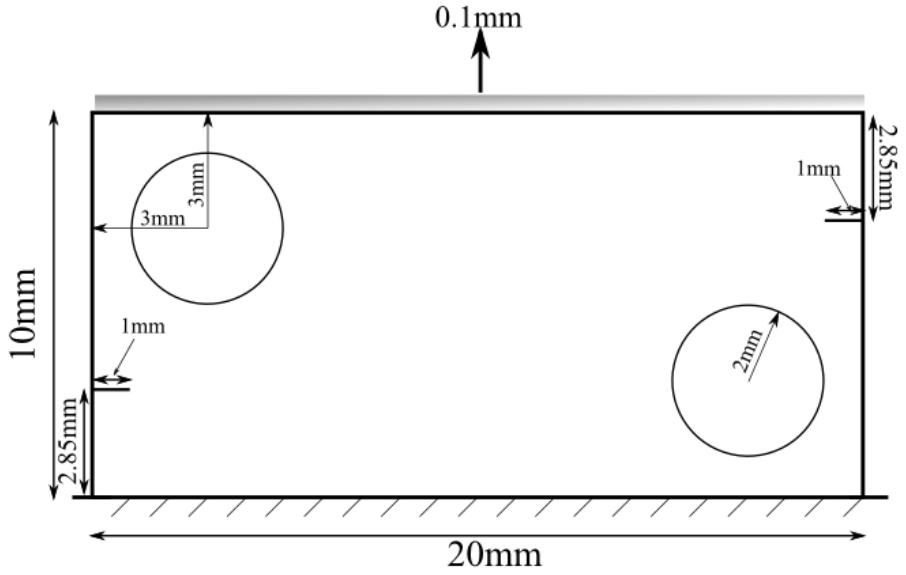

Fig. 34 Plate with two holes and two cracks subjected to tensile displacement.

Fig. 35 shows the crack paths, predicted by the present EFG method, are in good agreement with those obtained using FEM and XFEM. Initially, the crack is attracted by the nearest hole and then at a certain point, the two cracks are close enough to interact. This interaction effect leads to repulsion of the crack, which is well captured by the present method. Although the number of nodal degrees-of-freedom of the EFG method is significantly lower than that of the mesh-based methods, the results are accurate by virtue of the higher order continuous nature of the EFG shape functions. Furthermore, the nodal degrees-of-freedom are reduced by the usage of the diffraction methodology for kinked cracks.

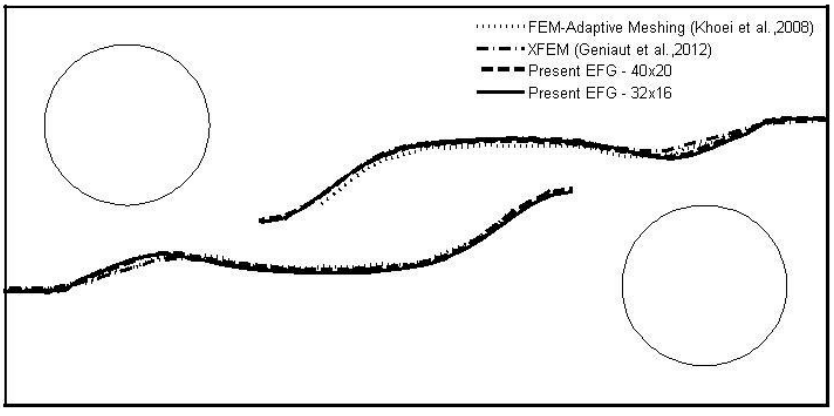

Fig. 35 Crack propagation in a plate with two holes.

8. CONCLUSIONS

The proposed variant of the EFG method integrates the use of level set method and diffraction methods for modelling multiple interacting cracks. This approach has been extended to model

kinked cracks that have knee singularity. The level sets for multiple cracks are extrapolated to a generic point through triangulation of nearest level set coordinates. These level sets are updated at each step of crack propagation. Based on the simulations, the following conclusions are drawn.

1. A very high nodal density is not required to obtain an accurate SIF of a crack interacting with neighbouring cracks using the proposed approach within the framework of EFG method. It is observed that even with coarser nodal density, the error is less than 1% and the solutions converged with increase in nodal density.
2. The proposed approach offers a computationally advantageous way of modelling crack propagation through step-by-step analysis.
3. The crack-crack interaction phenomenon scales the SIFs depending upon the proximity of the interacting crack tips. In the case of bi-material interface-subinterface crack interaction, the shielding and amplification effect of the energy release rate is observed.
4. The SIFs and energy release rate obtained using the interaction integral for various problems involving crack-crack and crack-microcrack interactions are in good agreement with the published results.

REFERENCES

[1] M. Kayama and N. Totsuka, "Influence of interaction between multiple cracks on stress corrosion crack propagation," Corrosion Science, vol. 44, pp. 2333-2352, 2002.

[2] M. Kayama and T. Kitamura, "A simulation on growth of multiple small cracks under stress corrosion," International Journal of Fracture, vol. 130, pp. 787-801, 2004.

[3] S. Darzens, J.L. Chermant, and J. Vicens, "Microcracking mechanism in a SiCf–SiBC composite creep-tested in argon," Journal of microscopy, vol. 20, pp. 230-237, 2001.

[4] H. Kebir, J.M. Roelandt, and L. Chambon, "Dual boundary element method modelling of aircraft structural joints with multiple site damage," Engineering Fracture Mechanics, vol. 73, pp. 418-434, 2006.

[5] M. Seyedi, S. Taheri, and F. Hild, "Numerical modeling of crack propagation and shielding effects in a striping network," Nuclear engineering and design, vol. 236, pp. 954-964, 2006.

[6] R.S. Barsoum, "On the use of isoparametric finite elements in linear fracture mechanics," Internatiional Journal of Numerical Methods in Engineering, vol. 10, pp. 25-37, 1976.

[7] S.K. Maiti, "A finite element for variable order singularities based on the displacement formulation," International Journal of Numerical Methods In Engineering, vol. 33, pp. 1955 - 1974, 1992.

[8] B.K. Dutta, S.K. Maiti, and A. Kakodkar, "Analysis of crack-microcrack inetractions and doubly kinked cracks using multiple singular points elements," Engineering Fracture Mechanics, vol. 38, pp. 215-223, 1991.

[9] S.K. Maiti, "A multicorner variable order singularity triangle to model neighbouring singularities," International Journal for Numerical Methods in Engineering, vol. 35, pp. 391-408, 1992.

[10] T. Belytschko and T. Black, "Elastic crack growth in finite elements with minimal remeshing," International Journal of Numerical Methods in Engineering, vol. 45, pp. 601-620, 1999.

[11] Moës. Nicolas, Dolbow. John, and Belytschko. Ted, "A finite element for crack growth without remeshing," International Journal of Numerical Methods in Engineering, vol. 46, pp. 1103-1118, 1999.

[12] C.A. Duarte and D.J. Kim, "Analysis and applications of a generalized finite element method with global–local enrichment functions," Computer Methods in Applied Mechanics and Engineering , vol. 197, pp. 487-504, 2008.

[13] V.P. Nguyen, R. Timon, B. Stéphane, and D. Marc, "Meshless methods: A review and computer implementation aspects," Mathematica and computers in simulation, vol. 79, pp. 763-813, 2008.

[14] T. Belytschko, Y.Y. Lu, and L. Gu, "Element-free Galerkin methods," International Journal of Numerical Methods in Engineering, vol. 37, pp. 229-256, 1994.

[15] T. Beltschko, L. Gu, and Y.Y. Lu, "Fracture and crack growth by element-free Galerkin methods," Modelling and Simulation Material Science Engineering , vol. 2, pp. 519-534, 1994.

[16] D. Organ, M. Fleming, T. Terry, and T. Belytschko, "Continuous meshless approximations for non-convex bodies by diffraction and transparency," Computational Mechanics, vol. 18, pp. 225-235, 1996.

[17] T. Rabczuk and T. Belytschko, "Cracking particles: a simplified meshfree method for arbitrary evolving cracks," International Journal for Numerical Methods in Engineering, vol. 61, pp. 2316-2343, 2004.
[18] G. Ventura, J.X. Xu, and T. Belytschko, "A vector level set method and new discontinuity approximations for crack growth by EFG," International Journal of Numerical Methods in Engineering, vol. 54, pp. 923-944, 2002.
[19] N. Muthu, S.K. Maiti, B.G. Falzon, and Yan Wenyi, "Crack Propagation in Non-homogenous materials: Evaluation of Mixed-Mode SIFs, T-stress and Kinking angle using a variant of EFG Method," Engineering analysis with boundary elements, vol. 72, pp. 11-26, 2016.
[20] M. Duflot and H. Nguyen-Dang, "A meshless with enriched weight functions for fatigue crack growth," International Journal for Numerical Methods in Engineering , vol. 59, pp. 1945-1961, 2004.
[21] M. Duflot, "A meshless method with enriched weight functions for three-dimensional crack propagation," International Journal for Numerical Methods in Engineering, vol. 65, pp. 1970-2006, 2006.
[22] I.V. Singh, B.K. Mishra, and P. Mohit, "A modified intrinsic enriched element free Galerkin method for multiple cracks simulation," Materials and Design, vol. 31, pp. 628-632, 2010.
[23] J. Shi, W. Ma, and N. Li, "Extended meshless method based on partition of unity for solving multiple crack problems," Meccanica, vol. 48, pp. 2263-2270, 2013.
[24] E. Barbieri, N. Petrinic, M. Meo, and V.L. Tagarielli, "A new weight-function enrichment in meshless methods for multiple cracks in linear elasticity," International Journal for Numerical Methods in Engineering, vol. 90, pp. 177-195, 2012.
[25] B. Muravin and E. Turkel, "Multiple crack weight for solution of multiple interacting cracks by meshless numerical methods," International Journal for Numerical Methods in Engineering, vol. 67, pp. 1146-1159, 2006.
[26] S. Osher and J.A. Sethian, "Fronts propagating with curvature dependent speed: algorithms based on Hamilton–Jacobi formulations," Journal of Computational Physics, vol. 79, pp. 12-49, 1988.
[27] J.A. Sethian, Level Sets Methods & Fast Marching Methods: Evolving Interfaces in Computational Geometry,Fluid Mechanics, Computer Vision and Materials Science. Cambridge, U.K.: Cambridge University Press, 1999.
[28] M. Stolarska, D.L. Chopp, N. Moës, and T. Belytschko, "Modelling crack growth by level sets in the extended finite element method," International Journal of Numerical Methods in Engineering, vol. 51, pp. 943-960, 2001.
[29] Z. Xiaoying, "Meshless methods: theory and application in 3D fracture modelling with level sets," School of Engineering and Computing Sciences, Durham University, PhD Thesis 2010.
[30] N. Moës, A. Gravouil, and T. Belytschko, "Non-planar 3D crack growth by the extended finite element and levelsets. Part I: Mechanical model," International Journal for Numerical Methods in Engineering, vol. 53, pp. 2549-2568, 2002.
[31] A. Gravouil, N. Moës, and T. Belytschko, "Non-planar 3D crack growth by the extended finite element and level sets. Part II: level set update," International Journal for Numerical Methods in Engineering, vol. 53, pp. 2569-2586, 2002.
[32] N. Sukumar, D.L. Chopp, and B. Moran, "Extended finite element method and fast marching method for three-dimensional fatigue crack propagation," Engineering Fracture Mechanics, vol. 70, pp. 29-48, 2002.
[33] N. Muthu, S.K. Maiti, B.G. Falzon, and I. Guiamatsia, "A comparison of stress intensity factors through crack closure integral and other approaches using eXtended element-free Galerkin method," Computational Mechanics, vol. 52, pp. 587-605, 2013.

[34] N. Muthu, S.K. Maiti, B.G. Falzon, and S. Khoddam, "Modified crack closure integral for extracion of SIFs in meshfree methods," Finite Element in Analysis and Design, vol. 78, pp. 25-39, 2014.
[35] P. Lancaster and K. Salkauskas, "Surfaces generated by moving least square methods," Mathematics of Computation, vol. 37, pp. 141-158, 1981.
[36] S. Mohammadi, XFEM fracture analysis of composites, 1st ed. Chichester, West Sussex: John Wiley and Sons, 2012.
[37] J.F. Yau, S.S. Wang, and H.T. Corten, "A mixed-mode crack analysis of isotropic solids using conservation laws of elasticity," Journal of Applied Mechanics, vol. 47, pp. 335-341, 1980.
[38] N. Sukumar, Z.Y. Huang, J.H. Prévost, and Z. Suo, "Partition of unity enrichment for bimaterial interface cracks," International Journal for Numerical Methods in Engineering, vol. 59, pp. 1075-1102, 2004.
[39] O.L. Bowie, "Rectangular tensile sheet with symmetric edge cracks," Journal of Applied Mechanics, vol. 31, pp. 208-212, 1964.
[40] Y.K. Cheung, C.W. Woo, and Y.H. Wang, "A general method for multiple crack problems in a finite plate," vol. 10, pp. 335-343, 1992.
[41] C. Daux, N. Moës, J. Dolbow, N. Sukumar, and T. Belytschko, "Arbitrary branched and intersecting cracks with the extended finite element method," International Journal for Numerical Methods in Engineering, vol. 48, pp. 1741-1760, 2000.
[42] M. Kachanov, "On crack-microcrack interactions," International Journal of Fracture, vol. 30, pp. 65-72, 1986.
[43] D. Ouinas, A. Hebbar, B.B. Bouiadjra, N. Benderdouche, and B. Serier, "Interaction effect crack-interfacial crack using finite element method," Materials and Design, vol. 31, pp. 375-381, 2010.
[44] S.K. Maiti and R.A. Smith, "Comparison of the criteria for mixed mode brittle fracture based on the preinstability stress-strain field Part I: Slit and elliptical cracks under uniaxial tensile loading," International Journal of Fracture, vol. 23, pp. 281-295, 1983a.
[45] S.K. Maiti and R.A. Smith, "Comparison of the criteria for mixed mode brittle fracture based on the pre-instability stress-strain field Part II: Pure shear and uniaxial tensile loading," International Journal of Fracture, vol. 24, pp. 5-22, 1983b.
[46] P.O. Bouchard, F. Bay, and Y. Chastel, "Numerical modelling of crack propagation: automatic remeshing and comparison of different criteria," Computer Methods in Applied Mechanics and Engineering, vol. 192, pp. 3887-3908, 2003.
[47] A.R. Khoei, H. Azadi, and H. Moslemi, "Modeling of crack propagation via an automatic adaptive mesh refinement based on modified superconvergent patch recovery technique," Engineering Fracture Mechanics, vol. 75, pp. 2921-2945, 2008.
[48] S. Geniaut and E. Galenne, "A simple method for crack growth in mixed mode with X-FEM," International Journal of Solids and Structures, vol. 49, pp. 2094-2106, 2012.